

# On the Post-Processing of Complex Additive Manufactured Metallic Parts: A Review


Shamim Pourrahimi and Lucas A. Hof<sup>\*</sup>

Additive manufacturing (AM) is gaining more attention due to its capability to produce customized and complex geometries. However, one significant drawback of AM is the rough surface finish of the as-built parts, necessitating post-processing for achieving the desired surface quality that meets application requirements. Post-processing of complex geometries, such as parts with internal holes, lattice structures, and free-form surfaces, poses unique challenges compared to other components. This review classifies various post-processing methods employed for complex AM parts, presenting the experimental conditions for each treatment alongside the resulting improvement in surface roughness as a success criterion. The post-processing methods are categorized into four groups: electrochemical polishing (ECP), chemical polishing (CP), mechanical polishing, and hybrid methods. Notably, mechanical methods exhibit the highest roughness improvement at 69.9%, followed by ECP (59.9%), hybrid methods (47.4%), and CP (49.5%). Nevertheless, mechanical post-processing techniques are less frequently utilized for lattice parts, making chemical or electrochemical methods more promising alternatives. In summary, all four categories of post-processing methods can improve the internal surfaces quality of AM holes. While mechanical methods offer the most substantial roughness improvement overall, chemical and electrochemical methods show particular potential for addressing the challenges associated with complex geometries.

## 1. Introduction

According to the International Organization for Standardization (ISO) and American Society for Testing and Materials (ASTM) definition, ISO/ASTM 52900, additive manufacturing (AM) refers to a fabrication method that involves the successive joining of materials to create physical object<sup>[1]</sup> and it is contrary to conventional subtractive manufacturing.<sup>[2]</sup> AM originated from the development of the patented stereolithography machine, which is recognized as one of the earliest three-dimensional (3D)

S. Pourrahimi, L. A. Hof  
Mechanical Engineering Department  
École de Technologie Supérieure  
1100, rue Notre-Dame Ouest, Montréal, Québec H3C 1K3, Canada  
E-mail: lucas.hof@etsmtl.ca

 The ORCID identification number(s) for the author(s) of this article can be found under <https://doi.org/10.1002/adem.202301511>.

© 2024 The Authors. Advanced Engineering Materials published by Wiley-VCH GmbH. This is an open access article under the terms of the Creative Commons Attribution License, which permits use, distribution and reproduction in any medium, provided the original work is properly cited.

DOI: 10.1002/adem.202301511

printers, dating back to 1986.<sup>[3]</sup> Since then, AM is gaining increased attention for functional part production because it offers design freedom,<sup>[4]</sup> which enables manufacturing complex geometric parts directly from computer-aided design (CAD) files that traditional manufacturing processes cannot produce. In addition, AM helps to reduce material consumption, chemical waste, process steps, and human resources.<sup>[5]</sup> Driven by these interesting characteristics, AM made an outstanding contribution in the biomedical, aerospace, automotive, and defense industries in recent years.<sup>[2,6,7]</sup>

A wide variety of AM processes have been proposed to create a 3D part from the supplied feedstock. Typically, for metal AM processes, feedstock consolidation into a dense part is required, which can be achieved by either melting or sintering.<sup>[2]</sup> Figure 1 illustrates the three most common AM processes for metals, namely powder bed fusion (PBF), direct energy deposition (DED), and binder jetting (BJ). This classification is based on the feedstock deposition method. Figure 1a shows a schematic of PBF technology, which includes all processes where

focused energy, either an electron beam or a laser beam, is used to sinter or melt a powder bed layer selectively. In this method, after spreading a thin layer of powder (typically size: 20–100 μm), some areas are selectively melted or sintered. The selective melting or sintering is repeated in a layer-by-layer fashion to build a final component.<sup>[8]</sup> Re-melting of previous layers during the melting of the current layer allows the adherence of the current layer to the rest of the part. Electron beam powder bed fusion (EB-PBF) machines are defined by deployment of an electron beam as power source for part fabrication. As such, laser beam powder bed fusion (LB-PBF) is using a laser as power source for powder fusion/sintering.<sup>[2,9]</sup>

DED encompasses AM processes where focused energy generates a melt pool into which feedstock is deposited (Figure 1b). This process can use a laser, arc, or electron beam as heat source and the feedstock can be either powder or wire. The origins of this category can be traced to welding technology, where materials are deposited outside a build environment by flowing a shielding gas over the melt pool.<sup>[2,10]</sup>

BJ is a layer-by-layer fabrication method, which works by depositing binder material in the designated regions of each powder (feedstock) layer, followed by curing of the binder

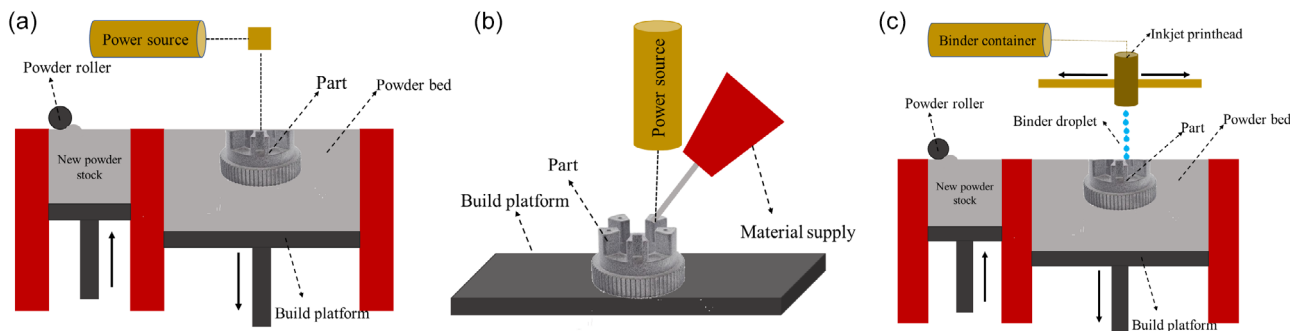


**Figure 1.** Schematic of most common AM methods for metals: a) PBF, b) DED, and c) BJ.

resulting in green part creation. In the next step, debinding and sintering are performed to eliminate the voids and enhance mechanical integrity.<sup>[2,11]</sup> A schematic of the binder deposition process is shown in Figure 1c.

For developing 3D metal components by AM, PBF is currently the most widely adopted method.<sup>[12–14]</sup> In literature, various names for the PBF method are typically utilized, including direct metal laser sintering (DMLS), laser powder bed fusion (LPBF), selective laser melting (SLM), selective laser sintering (SLS), and electron beam melting (EBM). However, the ISO-ASTM 52900<sup>[1]</sup> standard recommends the use of unified acronyms based on the production method rather than commercial names. Therefore, in this study, when laser is employed to produce metallic parts from a powder bed, it is referred to as LB-PBF, and when an electron beam is used for the same purpose, it is denoted as EB-PBF.

Compared with conventional manufacturing methods, AM parts typically possess poor surface quality characterized by highly irregular and randomly positioned features. These irregularities are created mainly due to the layer-by-layer nature of AM and the physical phenomena during deposition and fusion of feedstock.<sup>[15]</sup> In AM methods such as PBF and DED, which require high input energy, excess energy may result in overheating and semi-melted beads formation.<sup>[2,16]</sup> In PBF processes, EB-PBF parts have a lower level of dimensional accuracy and a rougher surface finish compared to LB-PBF parts due to a higher input energy.<sup>[2]</sup> For BJ, the amount of deposited binder affects the surface quality and geometric accuracy. Inadequate binder quantities (i.e., undersaturation) can cause the powder to drop easily from the green part, where excessive binder (i.e., oversaturation) may penetrate outside the designated area, resulting in poor surface finish and geometric accuracy deviation.<sup>[11]</sup>

Although AM is rapidly expanding as a practical production method to create complex 3D parts and lattice structures for many applications, their as-built quality poses challenges due to poor or inadequate surface finish for most final applications and this issue is even more severe for internal surfaces.<sup>[13,17–21]</sup> There are various ISO/ASTM standards on AM technology related to materials and processes, test methods, and design, but only about 4% are related to surface finishing on metal AM components.<sup>[22]</sup> As a result, in spite of its importance, surface quality is less considered in established AM standards for industry and academia.

Surface roughness refers to the unevenness of surface elevation present on a surface of an object<sup>[22]</sup> and surface roughness measurement is the method of quantifying the variations in the height of a physical object.<sup>[23]</sup> While a real surface topography is complex and cannot be completely described by a limited number of parameters, certain measurements are widely used in industry and research. The arithmetic average height ( $R_a$ ) is the most common parameter used to quantify surface roughness.<sup>[22]</sup> Since measurement and quantification of surface texture is essential for post-processing techniques and their evaluation, a more detailed introduction and discussion on surface texture and roughness parameters is provided in Section 2 of the present review paper.

**Figure 2** presents a schematic overview of the ranges of surface roughness produced by different commercially available PBF processes.

Among different imperfections leading to irregular surface morphology, we can mention the staircase effect due to the layer-by-layer nature of the deposition techniques, partially fused feedstock material (e.g., semi-melted beads), balling effects, spatter, or inadequate fusion.<sup>[15]</sup> Irregular or rough surfaces can hinder the performance of AM part, especially for components with internal channels or complex geometries, since it can affect fluid dynamics, heat transfer, optical properties, frictional properties,<sup>[14]</sup> and, more importantly, mechanical properties<sup>[17,24,25]</sup> and corrosion resistance.<sup>[26–29]</sup> Since most industries, such as biomedical and aerospace, require parts having smooth, shiny surfaces with low roughness, these issues significantly limit AM parts' application.<sup>[2,24]</sup>

Effective process parameters in the different AM technologies may control the resolution and surface finish of the end product. However, putting too much emphasis on these printing parameters to control the roughness is not useful for most applications, because it cannot guarantee a perfect surface roughness that meets the requirements of the end application. Hence, most metal AM parts ultimately require post-processing before functional use.

In general, post-processing methods can be divided into four categories: mechanical (abrasive), laser, chemical, and electrochemical.<sup>[12]</sup> External surfaces that are accessible by polishing tools or laser beams can be further smoothed by treatments such as mechanical or laser polishing.<sup>[30,31]</sup> In contrast, the post-processing options for complex AM parts are limited. In fact, methods in which the as-built AM part is submerged in

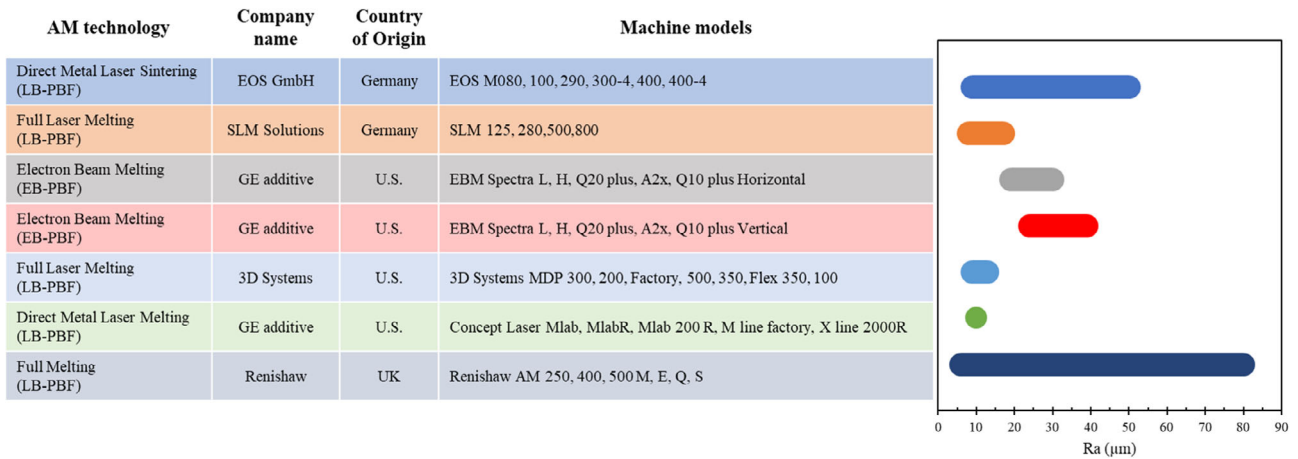


**Figure 2.** Surface roughness ( $R_a$ ) ranges produced by different, commercially available, PBF metal AM machines. Reproduced with permission.<sup>[23]</sup> Copyright 2020, Taylor & Francis.

a liquid, such as the case for chemical (CP) or electrochemical polishing (ECP), or methods in which a fluid including abrasive media can pass through the internal cavities are more promising for complex parts. In the context of this study, a *complex part* is defined as one with internal holes, channels, lattice structures, or free-form surfaces. **Figure 3** shows representative symbolic parts belonging to each of these categories.

The present article aims to review the advancements in surface modifications that can enhance the surface quality of complex metallic AM parts. Currently, scientific literature reports reviews on surface engineering of different alloys and AM parts, however, a thorough review of emerging strategies for AM *complex geometries* is not available. In light of the importance of surface treatment for AM parts and the overall surface

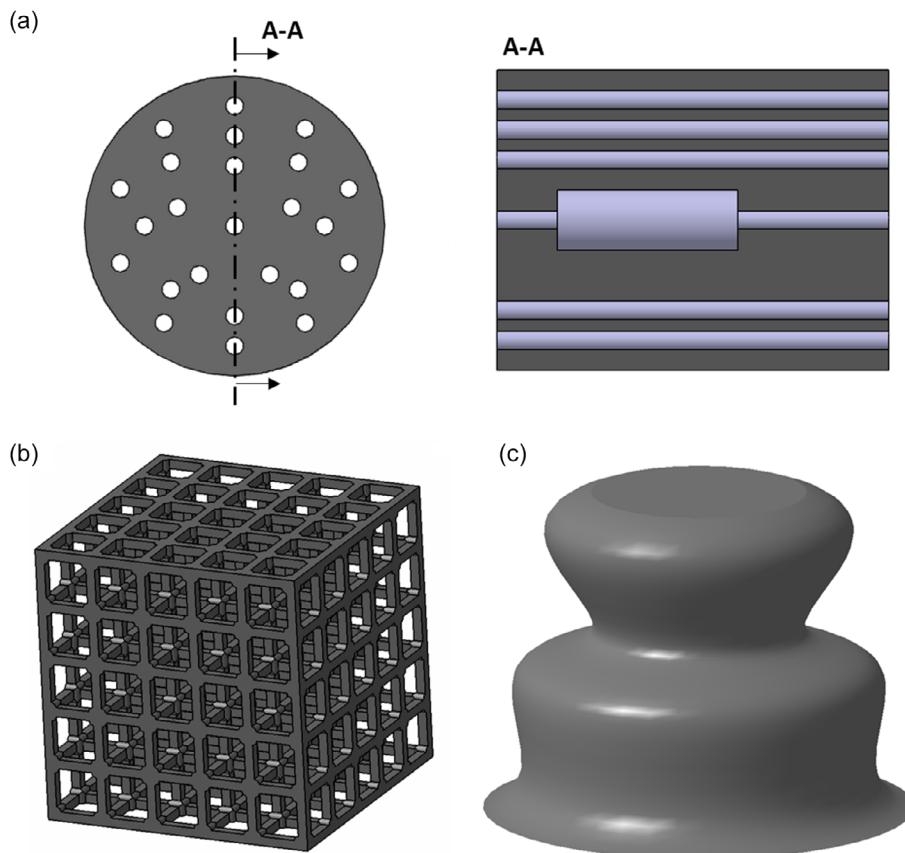


**Figure 3.** Symbolic representative of complex parts: a) internal holes, b) lattice structure, and c) free-form surface.

accessibility limitations in complex geometries, this article focuses on surface engineering of AM complex parts.

Firstly, Section 2 introduces and discusses various surface texture parameters and subsequently it presents typically deployed measurement technologies for complex parts' surface evaluation. Then, in the following sections, different post-processing methods are discussed, including details of the experimental condition and their results, notably ECP (Section 3), CP (Section 4), mechanical polishing (Section 5), and hybrid methods (Section 6). Each section concludes with a summary table including the details of part geometry and materials, post-processing experimental conditions, the maximum achieved roughness, and the amount of material removed by the experiment of each study. Finally, a comprehensive discussion including statistical analysis of each method is presented in Section 7 to help researchers and practitioners in the field of AM in finding the best post-processing option based on their part geometry and the desired roughness improvement. In addition, recommendations on future research directions in this area are provided, offering insights into potential advancements and areas for exploration within the AM community.

## 2. Surface Texture Evaluation

To compare the different post-processing techniques for complex metal AM parts, it is essential to introduce and discuss typical surface texture evaluation parameters and its measuring techniques. Section 2.1 introduces the parameters used to describe surface textures and Section 2.2 presents commonly deployed

surface texture evaluation technologies, including discussions on their strengths, limitations, and applicability.

### 2.1. Surface Texture Parameters

Texture parameters that describe the topology of a surface can be categorized into 2D parameters and/or 3D parameters. 2D parameters are known as profile parameters, while 3D parameters are known as areal parameters describing a surface. The application of 2D surface texture parameters in engineering and science dates back more than half a century.<sup>[22]</sup> Recently, there has been increased emphasis on the importance of 3D surface topography in both scientific and engineering applications. 3D roughness parameters are computed for a surface area rather than a singular profile, enabling them to provide a comprehensive representation of surface topology.<sup>[32]</sup>

The ISO standard outlined typically used surface texture parameters used in both industry and academia. ISO 21920-2<sup>[33]</sup> offers terms, definitions, and parameters for profile measurements, whereas ISO 25178-2<sup>[34]</sup> defines areal parameters. The parameters most commonly used or recommended for describing the surface texture of AM parts are listed in Table 1. However, it is important to note that the parameters used to describe the surface are not limited to those listed in Table 1. Many additional parameters are defined in standards such as ISO 2192-2 and ISO 25178-2, which are recommended for further reference.<sup>[33,34]</sup> In Table 1, the parameter name, description, and its formula as function of the spatial coordinates ( $x$ ,  $y$ , and  $z$ )

**Table 1.** Parameters describing surface texture in 2D or 3D according to standards ISO 21920-2<sup>[33]</sup> and ISO 25178-2,<sup>[34]</sup> respectively.

	Parameter	Description for a defined sampling length ( $l$ ) or area ( $A$ )	Formula	Used in
Profile texture parameters	$R_a$	Arithmetic means of absolute height values	$\frac{1}{l} \int_0^l  y(x)  dx$	[17,21,35–45]
	$R_q$	Root-mean-square value of height values	$\sqrt{\frac{1}{l} \int_0^l \{y(x)\}^2 dx}$	[43,44,46]
	$R_p$	Maximum height of the profile above the mean line	–	–
	$R_v$	Maximum height of the profile below the mean line	–	–
	$R_z$	Sum of the maximum peak height value and the maximum valley height value (average of 5l)	$R_p + R_v$	[35,37,40–44,50]
	$R_{sk}$	The skewness of a profile is the third central moment of profile amplitude probability density function	$\frac{1}{lR_q^3} \int_{-\infty}^{+\infty} v^3 p(v) dv$	–
	$R_{ku}$	Kurtosis coefficient is the fourth central moment of profile amplitude probability density function	$\frac{1}{lR_q^4} \int_{-\infty}^{+\infty} v^4 p(v) dv$	–
Profile texture parameters	$S_a$	Arithmetic means of the absolute of the ordinate values	$\frac{1}{A} \iint_A  z(x, y)  dx dy$	[13,19,20,40,41, 46–49]
	$S_q$	Root-mean-square value of the ordinate values	$\frac{1}{A} \iint_A z^2(x, y) dx dy$	[19,46]
	$S_p$	Largest peak height value	–	[19,46]
	$S_v$	Largest valley depth value	–	[19,46]
	$S_z$	Sum of the maximum peak height value and the maximum valley depth value	$S_p + S_v$	[19,40,46]
	$S_{sk}$	Quotient of the mean cube value of the ordinate values and the cube of $S_q$	$\frac{1}{S_q^3} \left[ \frac{1}{A} \iint_A z^3(x, y) dx dy \right]$	[46,47]
	$S_{ku}$	Quotient of the mean quartic value of the ordinate values and the fourth power of $S_q$	$\frac{1}{S_q^4} \left[ \frac{1}{A} \iint_A z^4(x, y) dx dy \right]$	[46]



are included. The schematics of 2D and 3D parameters are presented in **Figure 4** and **5**, respectively to support understanding their physical meaning.

The present review paper deployed a wide range of areal and texture parameters and also includes qualitative observations to assess the surface quality of the metal AM complex parts. **Figure 6a** provides a summary of the relative distribution percentages for areal texture evaluation, profile texture evaluation, combined areal and profile evaluations, and qualitative visual assessments as documented in the reviewed literature. **Figure 6a** shows that the predominant approach in the literature (39%) involves utilizing profile roughness parameters to characterize the surface texture of AM complex parts, while 29% of studies rely on areal roughness parameters. Approximately 25% of literature only used qualitative visual observation of scanning electronic microscopy (SEM) images or optical microscopy images. As well, 7% of studies employ a combination of both areal and profile roughness parameters for assessing surface texture. **Figure 6b** presents the frequency of each parameter utilized for the quantitative assessment of surface texture. The  $R_a$  surface roughness has been documented in 29% of the reviewed literature,<sup>[17,21,35–45]</sup> while the  $S_a$  parameter is used in 21%,<sup>[13,19,20,40,41,46–49]</sup> and  $R_z$  is used in 11%<sup>[35,37,40–44,50]</sup> of the reviewed literature studies. The rest of reported studies

(39%) have deployed other parameters for surface texture evaluation, which is further detailed in **Figure 6b**.

The reviewed literature indicates that there is no specific agreement on the selection of parameters for surface texture studies. However, the recently created standard guide ASTM F3624-23 Standard Guide for Additive Manufacturing Of Metals—Powder Bed Fusion—Measurement and Characterization of Surface Texture<sup>[51]</sup> has addressed this issue by providing optimal strategies and considerations for measurement and characterization of PBF surface textures. The standard encompasses a range of topics, including various surface measurement methods based on ISO 21920<sup>[33]</sup> and ISO 25178,<sup>[34]</sup> filtering methods, sample preparation techniques, and commonly used instruments for measuring metal PBF surface characteristics, among others.

According to ASTM F3624-23, a cutoff length of 2.5 mm is considered sufficient for profile measurements of PBF surfaces. Similarly, for areal measurements, considering a 2.5 mm × 2.5 mm area is recommended. Additionally, it is common practice to utilize L-filter nesting indices between 250 and 800 μm to extract weld tracks, smaller features, or both, present on the PBF surface for characterization. In profile-based analyses, it is suggested not to solely depend on the  $R_a$  parameter. Instead, it is suggested to utilize a comprehensive set of parameters

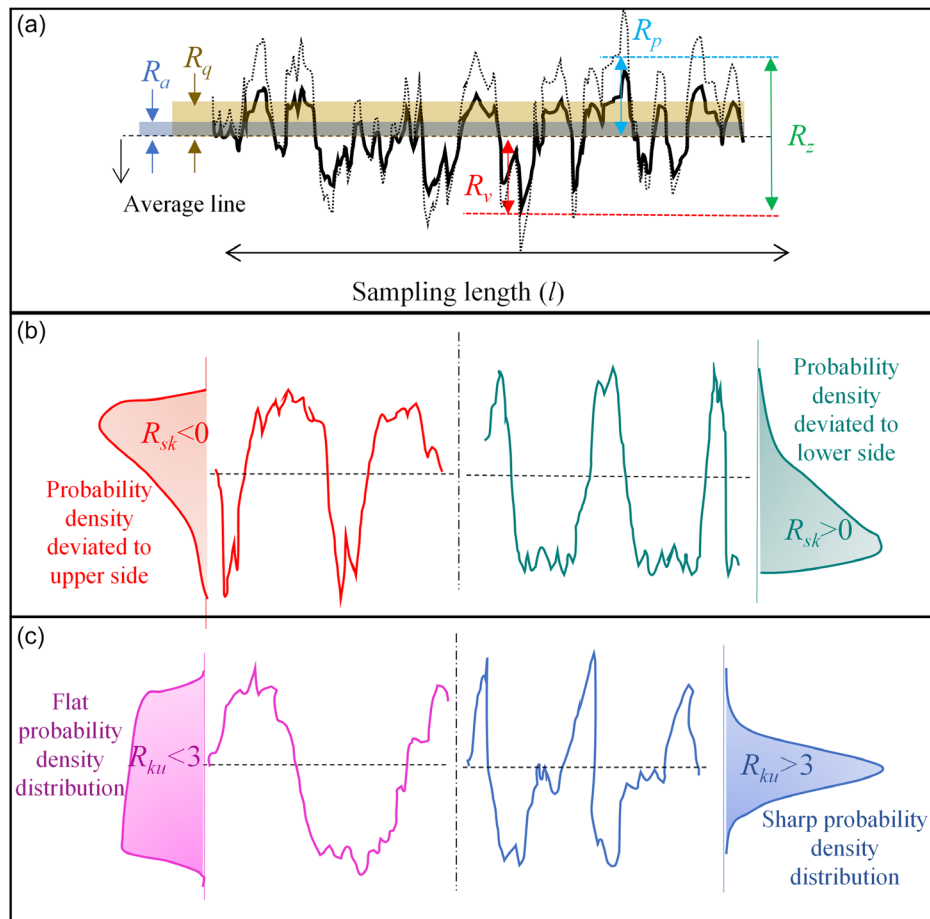


**Figure 4.** Schematic of the profile texture parameters: a)  $R_a$ ,  $R_q$ ,  $R_p$ ,  $R_v$ ,  $R_z$ , b)  $R_{sk}$  and the height probability distribution, c)  $R_{ku}$  and the height probability distribution.

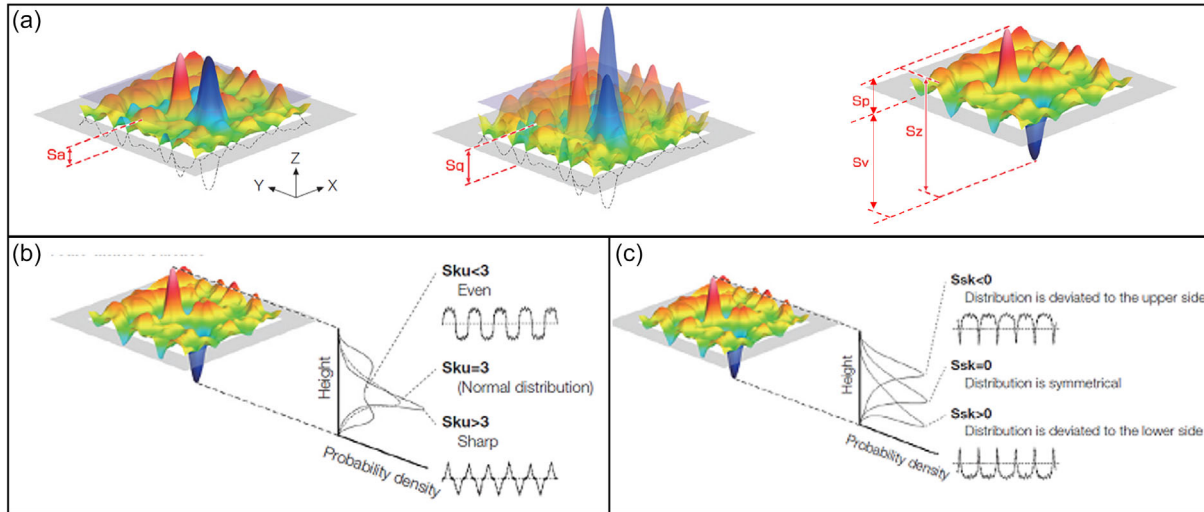


**Figure 5.** Schematic of the areal texture parameters: a)  $S_a$ ,  $S_q$ ,  $S_p$ ,  $S_v$ ,  $S_z$ , b)  $S_{sk}$  and the height probability distribution, and c)  $S_{ku}$  and the height probability distribution. Adapted with permission.<sup>[91]</sup> Copyright, Evident.

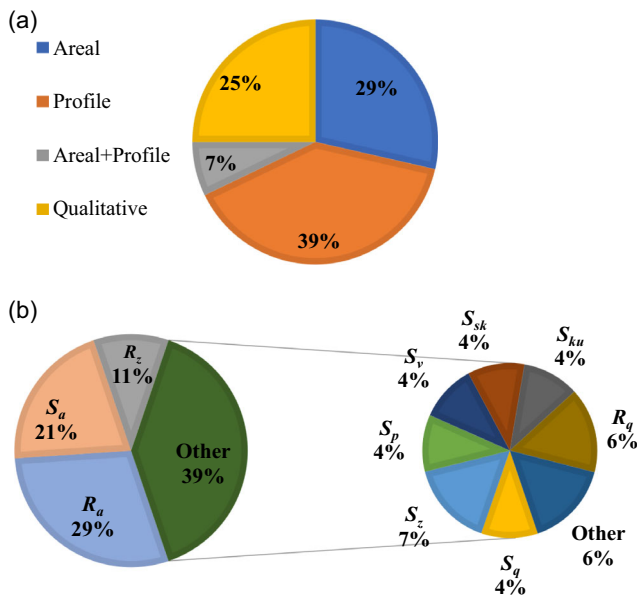


**Figure 6.** a) Pie chart illustrating the percentage of deployment for each surface texture evaluation parameter. b) Pie chart showing the frequency of use for quantitative parameters in the reviewed literature.

including  $R_a$ ,  $R_q$ ,  $R_z$ ,  $R_{sk}$ , and  $R_{ku}$ , along with parameters targeting peak features. Similarly, for areal measurements,  $S_a$ ,  $S_q$ , and  $S_z$  are frequently employed to evaluate surface texture for general assessment and comparison. However, these parameters typically only provide a statistical average. The incorporation of the skewness parameter  $S_{sk}$  can distinguish between upward-facing and downward-facing surfaces.<sup>[32,51]</sup>

## 2.2. Surface Measurement Technologies

While the parameters describing surface texture were introduced in Section 2.1, indeed, specific instrumentation is required to

extract these parameters. Among the most well-known and established technologies for measuring roughness, stylus profilometers can be identified. Williamson, Kubo, and Peklenik pioneered the introduction of this instrumentation and measurement method. A stylus profilometer operates by physically tracing the surface of a material with a fine stylus. As the stylus traverses the surface, it encounters variations in height, which are then translated into electrical signals. These signals are subsequently processed to generate a 2D profile of the surface, illustrating its roughness and texture. Subsequently, this concept has been extended to develop 3D stylus profilometers. In this method, the 3D map of the surface is obtained by tracing the stylus over several parallel profiles.<sup>[52,53]</sup> To utilize the stylus profilometry method for measuring surface roughness of complex parts, either only the external surface can be assessed,<sup>[39]</sup> or to access the internal surface, the part must be destroyed, making it a destructive analysis.<sup>[21]</sup>

Optical profilometry is a non-contact surface measurement technique used to characterize the topography of surfaces at micrometer or nanometer scales. It can be used to extract both profile and areal texture parameters and typically involves projecting structured light onto a surface and capturing its reflection. By analyzing the distortion of the projected pattern, precise measurements of surface features such as height, roughness, and texture can be obtained.<sup>[54,55]</sup> Although this method is non-contact, it requires surface exposure for characterization, or the parts need to be cut to characterize the internal surfaces.<sup>[19]</sup>

Another employed technique is focus variation microscopy, which was introduced by Danzl et al.<sup>[56]</sup> This approach involves an optical system with a limited depth of field coupled with vertical scanning. A series of images is captured as the optics moves vertically along the optical axis, producing a vertical stack of images. The variation of focus in each stack provides topographical and color information. This method is popular for measuring the surface topography of AM parts because it can capture high slope angles, while remaining relatively resilient to changes in optical properties such as reflectivity.<sup>[57]</sup> The depth of focus varies

depending on factors such as the magnification of the lenses, the wavelength of the light source, and the numerical aperture of the objective. If the surface of the complex part requiring characterization falls outside the depth of focus variation, then the part may need to be destructively analyzed to measure roughness.<sup>[47]</sup>

Laser confocal microscopy, developed by Sheppard et al.<sup>[58]</sup> in 1997, generates images by capturing reflected laser light from discrete focal planes. Similar to focus variation microscopy, a vertical motorized axis moves the laser up and down to enable focusing over a range of depths. The laser light reflected from the measured surface passes through a pinhole aperture positioned in front of a sensor, which detects alterations in surface elevation.<sup>[57]</sup> Similar to focus variation microscopy, laser confocal microscopy can serve as a non-destructive method for measuring roughness if only the target surface falls within the instrument's focus range. Alternatively, only the external area can be characterized; for example, in the case of a lattice structure, only the external struts can be characterized non-destructively.<sup>[46]</sup>

Micro-computed X-ray tomography (XCT) offers a non-destructive approach for characterizing internal features, particularly for surfaces inaccessible to conventional roughness measurement techniques. XCT enables the extraction of profile parameter data and subsequent analysis. In several studies, XCT data has been employed for conducting 2D analysis of surface profiles of complex parts.<sup>[35,36,59]</sup> However, recent investigations have shifted focus toward deriving equivalent areal parameters from XCT data, even though there is no specific emphasis on complex parts.<sup>[60,61]</sup> Consequently, a gap in research exists regarding the utilization of XCT for extracting areal parameters from complex parts.

**Table 2** summarizes the surface texture assessment technologies utilized in this literature review study. Indeed, it documents the methods used for quantitatively measuring profile roughness or areal roughness, as well as the literature that has evaluated roughness improvement through visual observation of SEM, optical, or XCT images.

It is important to note that parameters obtained from different technologies may not always align and provide similar results. According to Senin et al.<sup>[62]</sup> discrepancies between reconstructions can be notable, particularly for smaller scale features where local height differences are comparable to the feature being measured. However, larger-scale topographic formations generally

yield relatively consistent results. Moreover, it is essential not to perceive any of the illustrated measurement technologies as inherently superior or inferior when assessing metal PBF surfaces. The accuracy of results is heavily influenced by factors such as the instrument's make and model, current setup, and specific conditions related to the measured sample.<sup>[63]</sup>

Considering the reviewed literature on the post-processing of AM complex parts, it can be concluded that there was no specific consideration or rule in the reported literature studies, for selecting surface texture parameters and technologies. Instead, parameters and technologies were mostly chosen based on common utilization, such as the most well-known parameters like  $R_a$  or  $S_a$ , the preferences of the authors, or the availability of equipment. Considering the recently published standard, ASTM 3626, for selecting surface texture parameters and choosing appropriate measurement technologies can help to solve this issue. By integrating this standard into procedures within both industry and academia, a unified method can be developed for assessing surface texture in PBF parts. This unified effort will lead to the creation of a comprehensive and standardized database, thereby enhancing the comparability and reliability of research findings and industrial applications.

### 3. Electrochemical Polishing (ECP)

According to ASTM B374 definition, ECP improves the surface finishing of a metal by making the metallic part anodic in an appropriate (electrolytic) solution.<sup>[64]</sup> A schematic representation of a typical three-electrode ECP cell is indicated in **Figure 7a**. The working electrode (WE) acts as the anode, which is the workpiece to be polished. The counter electrode (CE), or auxiliary electrode, acts as the cathode to complete the electric circuit for current flow. The reference electrode (RE) allows reading the potential in the close vicinity of the WE, thereby reducing the disturbing effects of undesired potential drops by, for example, electrode polarization and electrolyte resistance, which are varying dynamically during the ECP process.<sup>[6,65–67]</sup> However, often in industrial and academic use simple two-electrode cells for ECP, omitting the RE, are deployed.<sup>[20,21,28,68,69]</sup> Among the distinguishing features of the ECP process are its contactless nature, use of electrical energy for accelerating the chemical reactions, and material removal irrespective of the hardness of the

**Table 2.** Summary of the surface texture assessment technologies used for surface texture characterizations of AM complex parts.

Surface texture assessment technologies		Part geometry	References
Profile measurement	Contact method	Stylus profilometer	Lattice, Internal cavity, Free-form, Internal cavity [17,21,37,39,41,42]
	Non-contact method	Confocal microscopy	Internal hole [40]
XCT		Lattice	[35,36,38]
Areal measurement	Non-contact method	Optical profilometry	Internal cavity, Lattice [19,48]
		Laser confocal microscopy	Internal hole, lattice [13,20,46,49]
		Focus variation microscopy	Internal hole [40,47]
2D/3D qualitative imaging	Non-contact method	Optical microscopy	Internal hole [27]
		SEM	Lattice [24,36,38,80,81,85]
		XCT	Lattice [92]

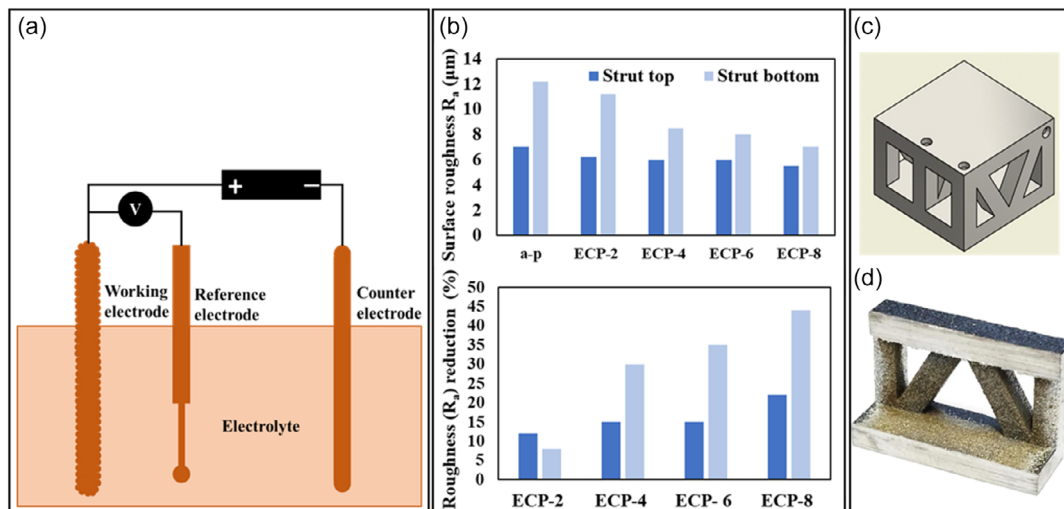


**Figure 7.** a) Schematic representation of a three-electrode ECP cell; b) Ti6Al4V lattice strut surface roughness measurement of the as-built and treated parts with different ECP duration, and the relative surface roughness reduction rates obtained. Reproduced with permission.<sup>[35]</sup> Copyright 2012, Wiley; c) Schematic of the lattice structure; d) Internal surface of the Ti6Al4V part after ECP at 50 V for 15 min. Adapted with permission.<sup>[21]</sup> Copyright 2019, Springer.

workpiece.<sup>[70]</sup> Electrochemical surface treatment methods can treat both internal and external surfaces in a complex structure, since fluid electrolytes can flow into internal parts and reach hidden surfaces.<sup>[13,21]</sup> ECP can be controlled by parameters such as potential (E), current density (i), temperature (T), electrolyte composition, ECP time, electrode distance, and electrolyte flow.<sup>[6]</sup>

It is worth mentioning that Equation (1) and (2) were used to calculate roughness improvement and thickness reduction throughout the present review study.

Roughness improvement %

$$= \frac{\text{Initial roughness} - \text{Final roughness}}{\text{Initial roughness}} \times 100\% \quad (1)$$

Thickness reduction %

$$= \frac{\text{Initial thickness} - \text{Final thickness}}{\text{Initial thickness}} \times 100\% \quad (2)$$

Literature reported the study of Pyka et al.<sup>[35]</sup> which deployed ECP for post-processing of a LB-PBF fabricated cylindrical lattice structure, having struts of 6 mm in diameter and 12 mm in height made of Ti6Al4V alloy. ECP was performed in a two-electrode cell in which the work piece was the anode and a cylindrical platinum basket (30 mm in diameter and 40 mm in height) was used as a cathode. The electrolyte composition was an aqueous solution containing 55 vol% CH<sub>3</sub>COOH + 30 vol% H<sub>2</sub>SO<sub>4</sub> + 15 vol% HF, and magnetic stirring was used to agitate electrolyte during the ECP treatment. ECP was performed under constant current density of 1.2 mA mm<sup>-2</sup> and four ECP times of 2, 4, 6, and 8 min were considered in their experiments. In this study, the surface roughness was measured for both top struts and bottom struts and their results are presented in Figure 7b. According to this figure, the best treatment was ECP for 8 min which decreased the surface roughness of top and bottom struts 22% (from  $R_a \approx 7 \mu\text{m}$  to  $R_a \approx 5.5 \mu\text{m}$ ) and

42% (from  $R_a \approx 12 \mu\text{m}$  to  $R_a \approx 7 \mu\text{m}$ ), respectively. Other surface roughness improvement and their values are presented in Table 3. Also, for the work reported by Pyka et al. no information was documented regarding the amount of material removed to improve the roughness; however, it is an important factor to control the change in dimensions through the post-processing.

In this study, roughness measurements were performed on 48 selected struts distributed uniformly through the lattice structure. Hence, this confirms that ECP can improve the surface quality of both internal and external struts and results in a homogenous roughness along with lattice height.<sup>[35]</sup> Despite this, the same observations did not appear in other, similar, studies. For example, Dong et al.<sup>[21]</sup> performed ECP on a Ti6Al4V lattice structure manufactured by LB-PBF which is schematically presented in Figure 7c. An alcohol-based electrolyte containing 995 mL ethanol, 100 mL n-butyl alcohol, 109 g of Al(H<sub>2</sub>O)<sub>6</sub>Cl<sub>3</sub>, and 250 g ZnCl<sub>2</sub>. Stainless steel (SS) was used as the CE with a distance of 5 mm from the WE. This study consisted of two ECP experiments, the first one applying a constant potential of 40 V for 10 min and the second applying a constant potential of 50 V for 15 min. Each experiment was repeated twice and the average improvement of external roughness was 11.49% (from  $R_a = 8.46 \mu\text{m}$  to  $R_a = 7.48 \mu\text{m}$ ) in the first experiment, and 36.06% (from  $R_a = 8.79 \mu\text{m}$  to  $R_a = 5.62 \mu\text{m}$ ) in the second experiment, as calculated using Equation (1). For internal surfaces, the roughness values were not reported, however, the average roughness improvement for both experiments are reported as -9%, hence an increase in roughness was noticed. Even though a layer of 75–100  $\mu\text{m}$  (equivalent to a 3–4% reduction in the initial strut thickness) was removed from the strut, it was performed from the external area only, resulting in no observed improvement for the internal surface. Figure 7d shows that the ECP process had no significant influence on the internal surface finish<sup>[21]</sup> and further explanations on the small increase in surface roughness of internal surfaces were not provided in this study.

**Table 3.** Summary of ECP experiments and their performance for AM complex parts.

Material	Electrolyte	Applied potential or current	Time	Other condition	Maximum roughness improvement (roughness values are in $\mu\text{m}$ )	Thickness reduction (relative and absolute)	References
Ti6Al4V (lattice)	55 mL CH <sub>3</sub> COOH + 30 mL H <sub>2</sub> SO <sub>4</sub> + 15 mL HF	1.2 mA mm <sup>-2</sup>	2 min	CE = Pt basket	11% ( $R_a$ : from 7 to 6.2)	–	[35]
			4 min	RE = NA	30% ( $R_a$ : from 12 to 8.8)	–	
			6 min		35% ( $R_a$ : from 12 to 8)	–	
			8 min		42% ( $R_a$ : from 12 to 7)	–	
Ti6Al4V (lattice)	995 mL ethanol, 100 mL n-butyl alcohol, 109 g of Al(H <sub>2</sub> O) <sub>6</sub> Cl <sub>3</sub> , and 250 g ZnCl <sub>2</sub>	40 V	10 min	CE = SS	–9%	3 $\approx$ 4%, 75 $\approx$ 100 $\mu\text{m}$	[21]
		50 V	15 min	RE = NA Working distance = 5 mm			
SS 316 (lattice)	60% H <sub>3</sub> PO <sub>4</sub> + 30% H <sub>2</sub> SO <sub>4</sub> + 0.3% Glycerol + 9.7% DI water	2.1 V	40 min	T = 50–60 °C CE = SS 316L sheet RE = SCE	–	–	[17]
SS 316 (internal hole)	2.4 M H <sub>2</sub> SO <sub>4</sub> + 5.9 M H <sub>3</sub> PO <sub>4</sub> + DI water	3.2 A cm <sup>-2</sup>	5 min	60 °C	–	–	[27]
Inconel 625 (internal hole)	80% H <sub>2</sub> SO <sub>4</sub> + Methanol	Wave: 30 V for 20 s, 0 V for 10 s	100 s	CE = SS RE = NA	Square: 64% ( $S_a$ : from 16.2 to 5.8) Round: 67% ( $S_a$ : from 15.2 to 5)	5%, 75 $\mu\text{m}$ 7%, 105 $\mu\text{m}$	[20]
SS 316 (internal cavity)	85% H <sub>3</sub> PO <sub>4</sub> + 15% H <sub>2</sub> SO <sub>4</sub>	60 A dm <sup>-2</sup>	30 min	T = 75 $\pm$ 2 °C Magnetic agitation = 200 rpm	–	–	[19]
Ti6Al4V (internal hole)	ethanol, isopropyl alcohol, AlCl <sub>3</sub> , and ZnCl <sub>2</sub>	70 V	350 s	Agitation=500 rpm Room temperature	Square bent flat: 83% ( $S_a$ : from 19.2 to 3.2) bent round: 60% ( $S_a$ : from 15 to 6),	14%, 140 $\mu\text{m}$ 8%, 80 $\mu\text{m}$	
SS 316 (internal hole)	60% H <sub>3</sub> PO <sub>4</sub> + 30% H <sub>2</sub> SO <sub>4</sub> + 0.3% Glycerol + 9.7% DI water	2.1 V + 1.7 V	20 min + 20 min	T = 50–60 °C CE = SS 316L sheet RE = SCE	–	70 $\mu\text{m}$	[17]
SS 17-4PH (lattice)	10 vol. H <sub>2</sub> SO <sub>4</sub>	4 $\approx$ 5 V	4 $\approx$ 5 min	CE = NA RE = NA	–	20 $\approx$ 60 $\mu\text{m}$	[71]
Inconel 718 (lattice)	COOLPULSE ES-C8020	7 V, 13 A	30 min	CE = IN 718 RE = NA	58% ( $S_a$ : from 26.4 to 10.9)	3.4%, 60 $\mu\text{m}$	[50]
Hastelloy X (internal hole)	Choline chloride and ethylene glycol 1:2 M ratio	30 V	5 min	CE = SS 316L mesh RE = NA T = 70 °C Magnetic agitation= 400 rpm	80% ( $R_a$ : from 22.3 to 4.5)	–	[43]
CoCr (lattice)	45 vol% H <sub>2</sub> SO <sub>4</sub> + 50% H <sub>3</sub> PO <sub>4</sub> + 5 vol% H <sub>2</sub> O	10 V, 2.1 A cm <sup>-2</sup>	3 min	CE = SS 316L T = 25 °C	85% ( $R_a$ : from 9.19 to 1.45)	–	[45]



Demir et al.<sup>[45]</sup> conducted ECP on an AM cardiovascular stent made of CoCr alloy produced by the LB-PBF method. The ECP process took place in a two-electrode cell using an electrolyte consisting of 45 vol% H<sub>2</sub>SO<sub>4</sub>, 50% H<sub>3</sub>PO<sub>4</sub>, and 5 vol% H<sub>2</sub>O and the CE used was made of SS316L. The process was carried out at room temperature for 3 min. This ECP treatment resulted in an 85% improvement of  $R_a$  surface roughness, decreasing it from 9.19 to 1.45  $\mu\text{m}$ . The cardiovascular stent's geometry consists of a single-layer tubular lattice structure rather than multiple grid-like layers. Therefore, the exposure of the workpiece to the CE was not a concern. As a result, ECP achieved a homogeneous and significant improvement in surface roughness.<sup>[45]</sup>

Jiang et al.<sup>[43]</sup> employed a deep eutectic solvent consisting of a eutectic mixture of choline chloride and ethylene glycol in a 1:2 molar ratio for the ECP of the nickel-based superalloy Hastelloy X. The part was an L-shaped cylindrical tube with a 3 mm diameter internal hole produced using LB-PBF and its cross section is shown in **Figure 8a**. The treatment was done in a two-electrode ECP cell at  $E = 30\text{ V}$  versus a SS 316L CE, at  $T = 70\text{ }^\circ\text{C}$ , with magnetic string 400 rpm for 5 min. The improvement in roughness of the internal hole was documented as 80%, decreasing from  $R_a = 22.3\text{ }\mu\text{m}$  to  $R_a = 4.5\text{ }\mu\text{m}$ . The surface texture improvement achieved by ECP is evident in the SEM image presented in **Figure 8a**, where the internal hole exhibits a shinier surface, with no attached partially melted particles visible in the cornering position. Despite the internal surface not being directly adjacent to the counter electrode, it has been well-polished. Such improvement was not observed in other studies using conventional

electrolytes.<sup>[19,21]</sup> This study demonstrates the effectiveness of emerging deep eutectic solvents as an ECP electrolyte.<sup>[43]</sup>

Tyagi and Manjaiah<sup>[71]</sup> employed ECP for surface treatment of sub-millimeter cell-sized (700  $\mu\text{m}$ ) SS 17-4PH TPMS (Gyroid, Diamond, and Schwarz) lattice structures. A potential in range of 4 to 5 V was applied for 4–5 min in a 10% H<sub>2</sub>SO<sub>4</sub> solution. Further details regarding the ECP cell were not documented. Surface texture evolution was observed through SEM images shown in **Figure 8b** by comparing the surface texture before and after ECP, which showed removal of the partially melted particles. However, quantitative analysis to measure roughness improvement was not conducted. Nevertheless, the struts' diameter was observed to decrease in the range of 20–60  $\mu\text{m}$ , due to material dissolution through ECP depending on the lattice type. The lattice type and the arrangement of voids can influence the mass transfer of ions during ECP, resulting in different thickness reductions. The highest thickness reduction of 60  $\mu\text{m}$  was identified for the Schwarz lattice, which exhibits less complexity compared to others.<sup>[71]</sup>

In summary, literature is generally lacking a reliable approach of ECP applied for internal surfaces, cavities, and complex AM parts, which require precise control of ECP conditions, since its performance is limited by the accessibility of the CE to the workpiece (WE).<sup>[13,20]</sup> According to the literature review, most promising ECP methods to improve the internal surfaces include 1) manipulating ECP potential or current density, and 2) implementing ECP using an inserted CE. The following Section 2.1 and 2.2 elaborate on each of these categories.

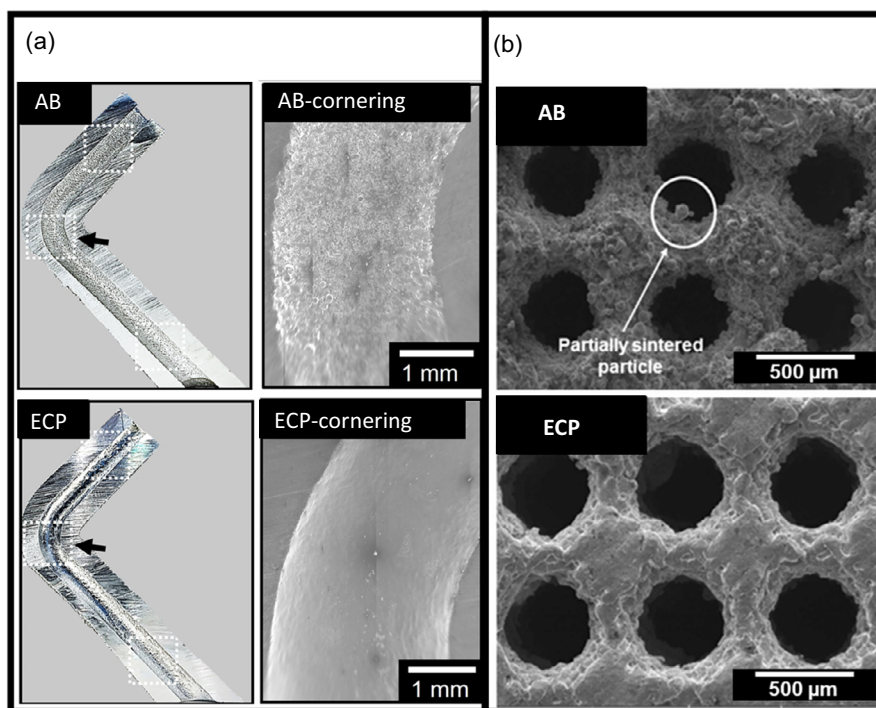


**Figure 8.** a) Sectioned view of a cylindrical tube and SEM image of the center cornering position in the as-built format (AB) and ECP. Adapted with permission.<sup>[43]</sup> Copyright 2022, Elsevier; b) Comparison between as-built (top row) and ECPed Schwarz TPMS structures. Circled areas with arrows indicate partially sintered particles that have been removed by ECP. Adapted with permission.<sup>[71]</sup> Copyright 2024, Elsevier.

### 3.1. ECP Potential and/or Current Density Variation Approaches

Several publications recommend ECP in the limiting current plateau region of polarization curves, as obtained for specific workpiece material and electrolyte combinations.<sup>[70,72,73]</sup> However, in this section, some non-traditional ECP strategies are introduced and discussed in detail for ECP of complex AM parts.

Chang et al.<sup>[17]</sup> used overpotential electrochemical polishing (OECP), i.e., ECP performed at higher potential ranges than indicated by the plateau region, to smoothen a SS316L lattice structure created by LB-PBF. The ECP was conducted at an elevated temperature (50–60 °C) in an electrolyte containing 60 vol% H<sub>3</sub>PO<sub>4</sub>, 30 vol% H<sub>2</sub>SO<sub>4</sub>, 0.3 vol% glycerol and 9.7 vol% deionized (DI) water. A three-electrode ECP cell, containing the work piece (WE), a 316L SS plate (CE), and a saturated calomel electrode (SCE) (RE) was used for the treatment. **Figure 9a** shows the electronic SEM images of the as-built and polished lattice structures that confirms the effectiveness of OECP. A very rough surface can be observed in **Figure 9a-A**, the as-built format of the lattice structure. After ECP for 40 min, applying a potential within the plateau region (around  $E = 1.7$  V vs. SCE) of the SS316 specific polarization curve, the structure shown in **Figure 9a-B** was obtained. It seems that the lattice surface is still rough, and some adhered particles are still visible, even if some struts were broken because of excessive and non-uniform polishing. On the other hand, ECP for 40 min in a higher range of potential (around  $E = 2.1$  V vs. SCE) showed a smooth surface, as indicated in **Figure 9a-C**. According to their measurements, a 150 μm reduction in strut diameter by OECP resulted in a smooth surface. No value for surface roughness of struts is reported, but according to their results, the surface quality improvement in both internal and external struts is visible.<sup>[17]</sup>

To effectively remove semi-melted beads, a higher current density is needed. Typically, the layer-by-layer texture on as-built parts is clearly visible, and this texture still appears after conventional ECP treatments at low current density. However, ECP at high current density promotes metal elution, resulting in more active dissolution of metals. In addition to improving the surface finish quality, a glossy effect can then also be achieved. Kim and Park<sup>[27]</sup> adopted this idea for post-processing of a SS316L LB-PBF cubic part with an internal hole, which is shown in **Figure 9b**. ECP was performed in a solution composed by 2.4 M H<sub>2</sub>SO<sub>4</sub> + 5.9 M H<sub>3</sub>PO<sub>4</sub> + DI water at a temperature of 60 °C, and constant current density of 3.2 A cm<sup>-2</sup> was applied for 5 min. **Figure 9b** shows optical camera images of this part before and after ECP. Roughness and thickness measurements were not performed for the internal surface of hole, however, according to the images, by ECP the surface became brighter and more reflective.<sup>[27]</sup>

In a study conducted by Ali et al.<sup>[20]</sup> a square waveform potential was applied for ECP on an Inconel 625 LB-PBF part. In this method, a potential of 30 V was applied for the duty cycle 20 s, followed by an interruption of 10 s with zero potential, which was repeated throughout the ECP process. The off-time was proposed to give the system sufficient time for agitation, removing surface contaminants, and cooling down the electrolyte. The electrolyte was 80 vol% H<sub>2</sub>SO<sub>4</sub> + 20 vol% CH<sub>3</sub>OH, and SS was used as the CE. This research studied the internal surface roughness improvement and thickness reduction for different shapes of square tube, round tube, and square bent tube samples. **Figure 9c** outlines the results of the ECP for 100 s. According to the roughness measurements reported in this study, the square, round, square bent flat, and square bent round tubes showed an internal surface roughness improvement of 64% (from  $S_a \approx 16.2$  μm to  $S_a \approx 5.8$  μm), 67% (from  $S_a \approx 15.2$  μm to

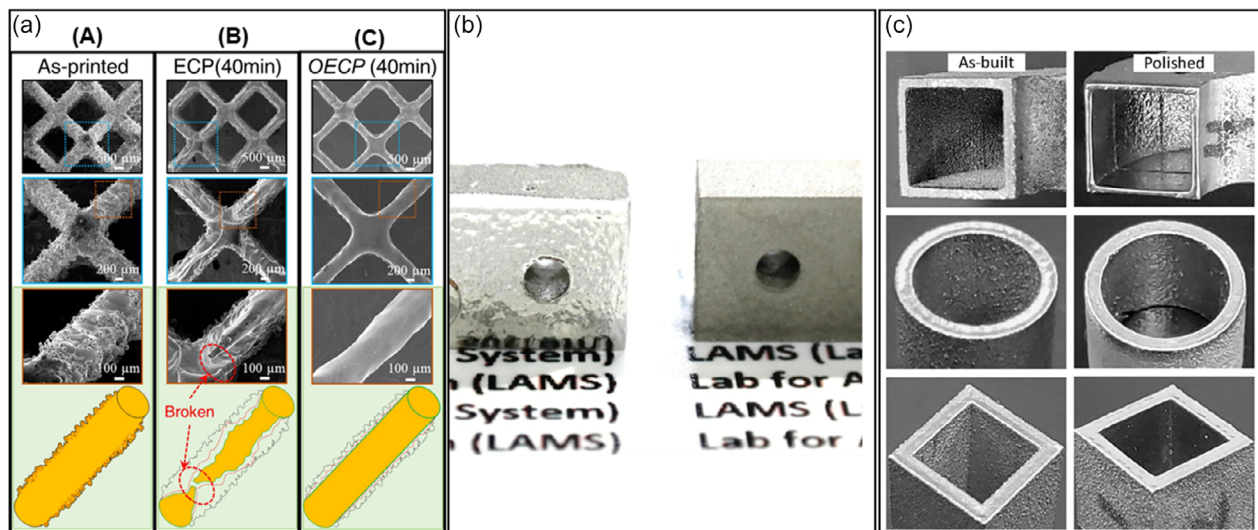


**Figure 9.** a) Smoothing of AM body-centered-cubic (BCC) lattice surface by conventional ECP versus novel OECP A) As-printed rough lattice surface with sticking particles B) after conventional ECP for 40 min C) after novel OECP. Adapted under the term of the CC BY 4.0.<sup>[17]</sup> Copyright 2019, The Authors. Published by Taylor & Francis; b) Optical image of SS316 part comparing surface reflection before (right) and after (left) ECP. Adapted with permission.<sup>[27]</sup> Copyright 2019, Springer; c) As-built (left column) and polished (right column) Inconel parts. Adapted with permission.<sup>[20]</sup> Copyright 2020, Elsevier.

$S_a \approx 5 \mu\text{m}$ ), 83% (from  $S_a \approx 19.2 \mu\text{m}$  to  $S_a \approx 3.2 \mu\text{m}$ ) and 60% (from  $S_a \approx 15 \mu\text{m}$  to  $S_a \approx 6 \mu\text{m}$ ), respectively, with a thickness reduction of  $75 \mu\text{m}$  (5%),  $105 \mu\text{m}$  (7%),  $140 \mu\text{m}$  (14%), and  $80 \mu\text{m}$  (8%), respectively.<sup>[20]</sup> According to the reviewed literature in this section, performing ECP on higher levels of potential or current density enables to extend effective surface finishing by ECP to internal surfaces.

### 3.2. ECP of Internal Surfaces Using Inserted Cathode

Although ECP is an effective post-processing method, the application of ECP in complex geometries is limited by the availability of the CE. This issue can be addressed by inserting the cathode material into the complex part to try keeping a more uniform WE-CE distance for the full part's surface. This method can be used to post-process the internal part of holes and is not limited to holes in AM parts.<sup>[74,75]</sup> Several researchers and industries, such as Extrude Hone Corporation,<sup>[76]</sup> insert the additively manufactured CE into the holes, or other accessible inner features, of a complex part to polish internal surfaces. Tyagi et al.<sup>[19]</sup> also demonstrated the accessibility issue and the effect of an inserted CE on ECP surface finish performance of internal surfaces in SS316 LB-PBF fabricated components. Two types of samples were studied that are shown in **Figure 10a**. The opening diameter of type 1 is 2 mm, while the opening diameter of type 2 is 10 mm with the ability to insert a CE. ECP was performed in an acidic solution containing 85 vol%  $\text{H}_3\text{PO}_4$  and 15 vol%  $\text{H}_2\text{SO}_4$  at a temperature of  $75 \pm 2^\circ\text{C}$ . To prevent the ECP product from

agglomerating near the AM surface, an electromagnetic stirrer at 200 rpm was used to agitate the electrolyte. Constant current density of  $60 \text{ A dm}^{-2}$  was applied for 30 min to polish the parts. Lead (Pb) was used as a screw-like CE inserted into a hole during the experiments for sample type 2, as indicated in **Figure 10a**. The external surfaces became shiny for both sample types. The internal surfaces of the parts after ECP are shown in **Figure 10b**. According to **Figure 10b**, since the internal surface of type 1 was not exposed to the CE, the surface seems dull and its quality did not show any improvement; whereas, for type 2, since the CE was inserted into the hole, a shiny surface was obtained after ECP. Optical profilometry was used to perform the quantitative analysis of surface roughness evolution. The  $S_a$  for external unpolished surface was  $13.88 \pm 2.65 \mu\text{m}$ , which decreased to  $3.0 \pm 0.75 \mu\text{m}$  for both type 1 and type 2. The initial surface roughness of internal surfaces was not reported, but the final  $S_a$  value for type 2 was reported to be  $20 \pm 10 \mu\text{m}$ . Hence, based on the given information, visual evaluations can confirm the effectiveness of insertable CEs, but no quantitative improvement can be assessed.<sup>[19]</sup>

In a study by Fayazfar et al.<sup>[13]</sup> the CE was produced simultaneously with the workpiece, using additive manufacturing. Hence, the CE shape matches with the WE, as is shown in **Figure 10c**. In this study, the ECP of Ti6Al4V complex structures was conducted in a non-aqueous electrolyte with a mixture of ethanol, isopropyl alcohol,  $\text{AlCl}_3$ , and  $\text{ZnCl}_2$ , at room temperature and magnetic stirring with a speed of 500 rpm. An electrochemical pulse polishing, with a repetitive 20 s “on” and 10 s

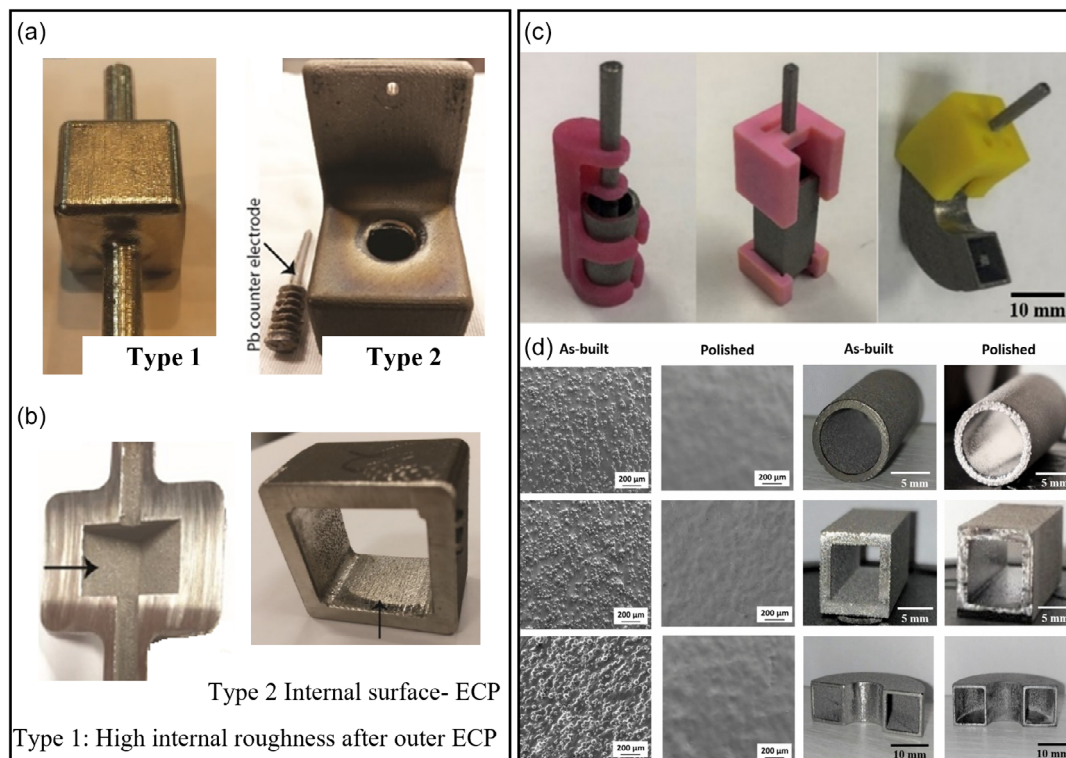


**Figure 10.** a) SS316 parts with internal cavities; b) Internal surfaces after ECP. Adapted with permission.<sup>[19]</sup> Copyright 2018, Elsevier. c) Ti6Al4V parts (WE/CEs) with polymer 3D-printed fixture; d) SEM micrographs of as-built and electropolished samples with various geometries with optical images of as-built and electropolished samples. Adapted with permission.<sup>[13]</sup> Copyright 2021, ASM International.



“off”, was used to electropolish the parts. In other words, two strategies of “insertion of cathode electrode” and “application of artificial waveform potential” were adapted to make the internal surface smooth. An industrial ECP system from ESMA Inc. (South Holland, IL) was used in this study. Both WE and CE were made of Ti6Al4V and the potential of 70 V was applied for ECP. ECP time for rectangular and cylindrical parts were 350 sec and 800 sec for the U-shape because of its higher initial roughness ( $S_a = 32.4 \mu\text{m}$ ). To observe the effectiveness of ECP, the  $S_a$  surface roughness parameter and thickness loss were measured, confirming significant surface improvement with low thickness reduction for all samples in this ECP method. The cylinder, rectangular, U-shape flat and U-shape curved samples showed a decrease in surface roughness of 76.5% (from  $S_a = 14.02 \mu\text{m}$  to  $S_a = 3.29 \mu\text{m}$ ), 64.6% (from  $S_a = 14.21$  to  $S_a = 5.03 \mu\text{m}$ ), 70.6% (from  $S_a = 14.96$  to  $S_a = 4.4 \mu\text{m}$ ), and 36.4% (from  $S_a = 32.4$  to  $S_a = 20.6 \mu\text{m}$ ), respectively, and thickness loss of 7%, 5%, 12% and 8%, respectively. Note that the as-printed curved surface of the U-shape part was rougher ( $S_a = 32.4 \mu\text{m}$ ) than the flat side ( $S_a = 14.9 \mu\text{m}$ ). This is typical in LB-PBF downward-facing (down-skin) surfaces due to the different laser-material interaction phenomena.<sup>[77,78]</sup> i.e., a smaller surface roughness value ( $S_a = 4.4 \mu\text{m}$ ) was measured on the flat side of the U-shape tube compared to the curved side ( $S_a = 20.6 \mu\text{m}$ ). Furthermore, due to a higher degree of electrolyte agitation, the internal surface roughness of the cylinder sample after ECP was lower than the rectangular part as validated by optical and SEM images (Figure 10d). The thickness reduction associated with the roughness improvement for all geometries is reported in Table 3.<sup>[13]</sup>

Lynch et al.<sup>[50]</sup> have used the same idea of an inserted CE for ECP of lattices made of Inconel 718. The lattices and CE were printed by the LB-PBF method with similar materials. The commercial process COOLPLUSE was used with the electrolyte COOLPULSE ES-G8020 for the ECP treatment. As indicated in Figure 11a, the COOLPLUS tooling consists of two parts: an outer cathode and an inner cathode. The inner cathode consists of several tubes with featured openings at their ends, enabling continuous flushing of electrolyte around the exterior and into the interior of the lattice specimen. A potential difference of 7 V was applied between the WE and the CE inserted for 30 min to maintain a current of 13 A for ECP. The treatment effectively improved the surface roughness by up to 58%, reducing  $S_a$  from 26.4  $\mu\text{m}$  to 10.9  $\mu\text{m}$ . This improvement was achieved through material dissolution, which decreased the strut thickness by 3.4% (i.e., down to 60  $\mu\text{m}$ ).<sup>[50]</sup>

Generally, this type of cathode electrode insertion is highly geometry dependent, and for each workpiece, an individual cathode electrode should be printed. Hence, this approach adds significantly to the part’s manufacturing cost and material (feed-stock) consumption, thus increasing the production method’s carbon footprint.<sup>[79]</sup> Another type of cathode that can be installed inside pipes is shown in Figure 11b. This model is more flexible and less dependent on geometry. Chang et al.<sup>[17]</sup> proposed these 3D-printed electrodes for polishing internal surfaces more efficiently and controllably. Figure 11b shows a series of electrodes with customized shapes for polishing internal surfaces of curved pipes. 3D-printed electrodes can be placed according to the requirements at any point, even local polishing can be accomplished. Two typical pipe structures were selected for

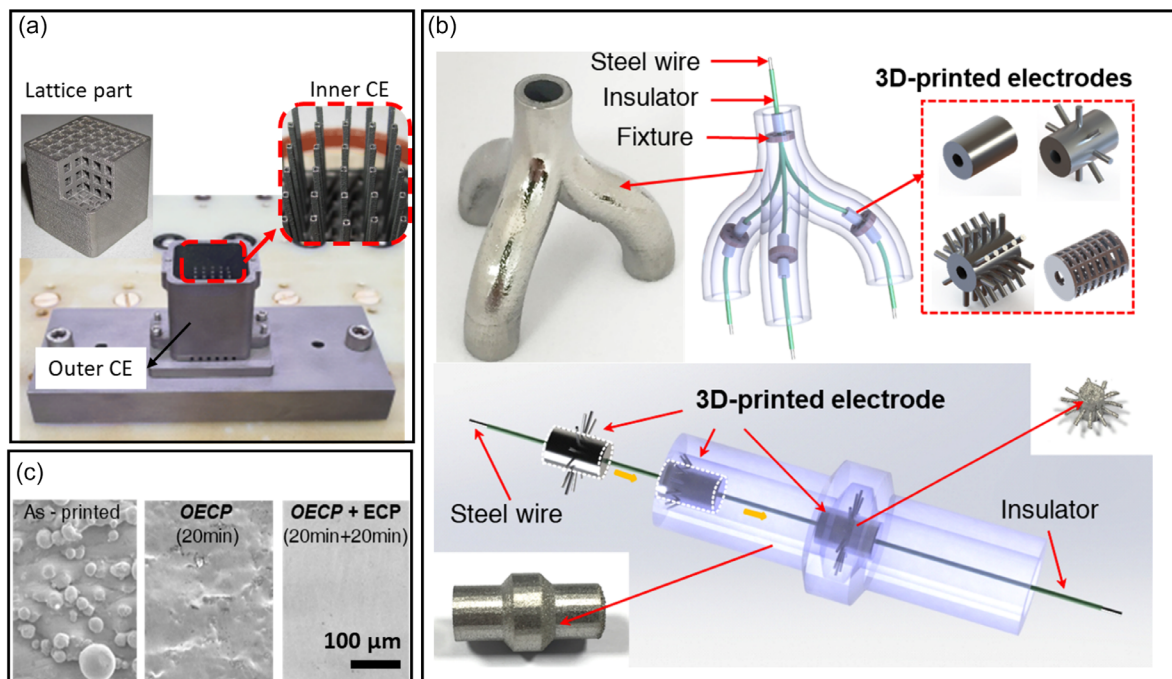


**Figure 11.** a) Internal and external AM CE for lattice part. Adapted with permission.<sup>[50]</sup> Copyright 2021, Springer. b) Cathode electrodes fabricated by 3D-printing for ECP of pipe’s internal surface with constant-diameter and variable-diameter; c) Internal surface improvement of the curved pipe after a combination of OECP and ECP. Adapted under the terms of the CC BY 4.0.<sup>[17]</sup> Copyright 2019, The Authors. Published by Taylor & Francis.

polishing, a curved pipe with constant diameter and a pipe with variable diameter. The pipes were made of SS316L and produced by LB-PBF. At an elevated temperature (50–60 °C), ECP was conducted in an electrolyte containing 60 vol% H<sub>3</sub>PO<sub>4</sub>, 40 vol% H<sub>2</sub>SO<sub>4</sub>, 3.3 vol% Glycerol, and 9.7 vol% DI water. A three-electrode ECP cell was used, in which SS316L plate served as the CE and SCE was used as the RE. In ECP, a constant potential of around 2.1 V was used. As can be seen in Figure 11c, the smooth internal surface of pipes was achieved by combining OECP and ECP processes, using designable electrodes. The study does not report ECP parameters or roughness and thickness measurements.<sup>[17]</sup>

The summary of all literature reviewed in this section is presented in Table 3 that outlines the material, the ECP electrolyte, applied potential or current, time, and the type of the used CE or RE in different columns. In the last three columns, the roughness improvement as well as the thickness reductions are listed. In case of unavailable information regarding the processing parameters, it is mentioned as NA.

#### 4. Chemical Polishing (CP)

CP, also known as chemical etching, is another post-processing method to mitigate the surface roughness of as-built AM parts. In CP, the metallic part is immersed in a chemical solution bath, under a temperature-controlled condition, for a specific duration to make the surface bright and aesthetically pleasant.<sup>[15]</sup> According to Tyagi et al.<sup>[19]</sup> CP of SS316 LB-PBF components was effective in both reducing the internal and external roughness. To perform CP treatment the parts were immersed in DS-9314 commercial solution at temperature of  $T = 75 \pm 2$  °C for 30–90 min. In their work, the internal and external surface roughness were improved by about 62%, from  $S_a = 13.88 \pm 2.66$  μm to  $S_a = 5.22 \pm 2.46$  μm. This study concluded that CP could be applied to any complicated AM shape and geometry. Figure 12a,b show the texture of the part after CP. Figure 12c,d illustrate the SEM morphology observations of parts before and after CP.<sup>[19]</sup>

In another study, Pyka et al.<sup>[36]</sup> have employed a full-factorial design of experiment (DOE) on a LB-PBF fabricated Ti6Al4V part

featuring an open porous structure. In this experiment, the etching time and the chemical etching solution concentration were investigated in relation with the achieved surface roughness. According to their results, the concentration of the surface treatment solution (HF + H<sub>2</sub>O) was the most important factor for reducing roughness efficiently. The best CP condition of the part in their study was a treatment with a 1.1 wt% hydrogen fluoride (HF) solution for 14 min, which reduced the surface roughness from  $R_a \approx 26.7$  μm down to  $R_a \approx 8$  μm. Figure 12e,f present the struts of the titanium alloy AM part investigated in this study, before and after CP, respectively. The surface roughness measurements, before and after treatments, are based on micro-computerized tomography (micro-CT) 3D scan visualizations, which are illustrated in Figure 12g and h. No information was documented regarding the struts' thickness change by the CP treatment.<sup>[36]</sup>

Another study using CP, conducted by Karami et al.<sup>[24]</sup> concentrated on improving the internal and external surface roughness of LB-PBF produced Ti6Al4V lattice structures. They used two routines for the CP process: (CP1) AM part treatment for 120 s under ultrasonic agitation in a solution containing 50 mL H<sub>2</sub>O + 25 mL HNO<sub>3</sub> + 5 mL HF and (CP2) AM part processing for 60 min under ultrasonic agitation in a solution containing 50 mL H<sub>2</sub>O + 25 mL H<sub>2</sub>SO<sub>4</sub> + 25 mL HCl. Compared with the first chemical solution (CP1), which contained HF, the second chemical solution (CP2) was less hazardous and performed the polishing well. In their study, the principal objective was to explore the effect of post-processing on the mechanical performance of the parts, hence surface roughness and thickness measurements results were not reported. However, the microscopic characterizations revealed that CP could penetrate deep into the lattice structure, remove the adhered particles, and improve the surface quality.<sup>[24]</sup>

Mohammadian et al.<sup>[37]</sup> have removed semi-melted particles and improved the surface roughness of an Inconel engine part produced by LB-PBF with an internal edge shape cavity by using the flow of a chemical solution. In such a chemical flow polishing process, the metal dissolution enhances with an increased flow velocity. Therefore, the flow can accelerate part treatments compared to CP in a static solution. In a first step of this study, CP in

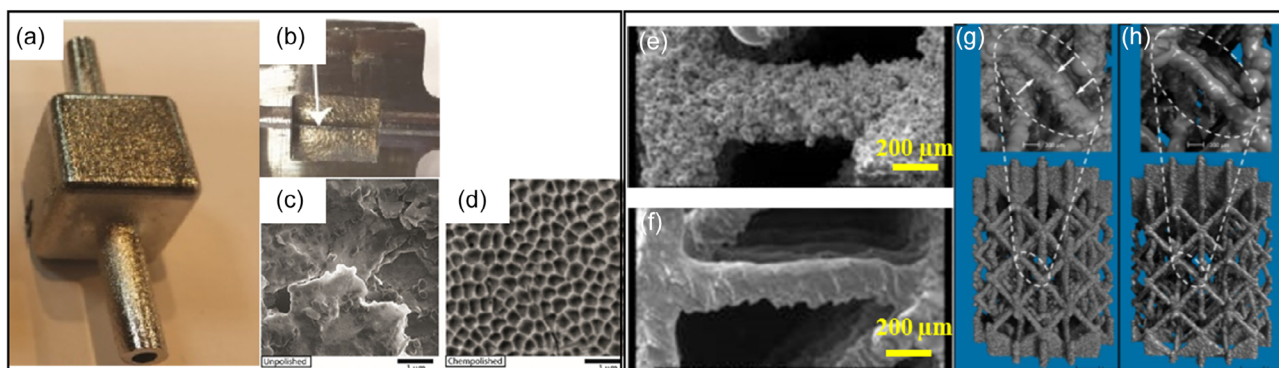


**Figure 12.** Optical image of a) external and b) internal AM SS316 part after CP. SEM study of c) unpolished, d) chemically polished of same part. Adapted with permission.<sup>[19]</sup> Copyright 2018, Elsevier. SEM micrographs of e) as-produced and f) surface-treated as well as Micro-CT-based 3D visualizations g) before and h) after CP treatment of Ti6Al4V open porous structure. Adapted under the terms of the CC BY 3.0.<sup>[36]</sup> Copyright 2013, The Authors. Published by MDPI.



**Table 4.** Summary of CP experiments and their performance for AM complex parts.

Material	Electrolyte	Time	Other conditions	Max roughness improvement (roughness values are in $\mu\text{m}$ )	Thickness reduction (relative and absolute)	References
SS316 (internal cavity)	DS-9-314 (10%–30% $\text{H}_3\text{PO}_4$ , 1%–10% $\text{HCl}$ , 1%–10% $\text{HNO}_3$ , and 1%–10% proprietary surfactants)	30–90 min	$T = 75 \pm 2^\circ\text{C}$	62% ( $R_a$ : from 13.88 to 5.22)	–	[19]
Ti6Al4V (lattice)	1.1% $\text{HF} + \text{H}_2\text{O}$  0.5% $\text{HF} + \text{H}_2\text{O}$	10 min	–	36% ( $R_a$ : from 15.6 to 10)	–	[36]
		14 min	–	70% ( $R_a$ : from 26.7 to 8)	–	
		10 min	–	35% ( $R_a$ : from 13.8 to 9)	–	
		14 min	–	53% ( $R_a$ : from 19.1 to 9)	–	
Ti6Al4V (lattice)	50 mL $\text{H}_2\text{O} + 25\text{ mL HNO}_3 + 5\text{ mL HF}$ 50 mL $\text{H}_2\text{O} + 25\text{ mL H}_2\text{SO}_4 + 25\text{ mL HCl}$	2 min	–	–	–	[24]
		60 min	–	–	–	
Inconel 625 (internal cavity)	50% $\text{HF} + 50\% \text{HNO}_3$	1 h	Flow rate = $10\text{ L min}^{-1}$ $T = 25^\circ\text{C}$ $T = 25^\circ\text{C}$	23% ( $R_a$ : from 7.3 to 5.6)	50 $\mu\text{m}$	[37]
				4% ( $R_a$ : from 7.3 to 7)	–	
				39% ( $R_a$ : from 7.3 to 4.1)	–	
	64.5% $\text{CH}_3\text{COOH}$ (ice cooled) + 35% $\text{HNO}_3 + 0.5\% \text{HCl}$ 30% $\text{HF} + 70\% \text{HNO}_3$ 30% $\text{HNO}_3 + 10\% \text{H}_2\text{SO}_4 + 10\% \text{H}_3\text{PO}_4 + 50\% \text{CH}_3\text{COOH}$	8 h	–	15% ( $R_a$ : from 7.3 to 6.2)	–	–
				12% ( $R_a$ : from 7.3 to 6.4)	–	
				1.3% ( $R_a$ : from 7.3 to 7.2)	–	
Ti (Gr. 1) (lattice)	1.3% $\text{HF}/9.0\% \text{HNO}_3$	3–18 min	–	–	10 $\approx$ 25%, 15 $\approx$ 60 $\mu\text{m}$	[81]
Ti6Al4V (lattice)	3% $\text{HF} + 13\% \text{HNO}_3 + \text{H}_2\text{O}$	4 $\times$ 30 min	–	27% ( $R_a$ : from 34.3 to 24.8)	–	[38]
Ti6Al4V (lattice)	0.5 mL $\text{HF} + 50\text{ g H}_2\text{O}$	10 min	–	17% ( $R_a$ : from 12 to 10)	13%, 29 $\mu\text{m}$	[35]
Pure Zn	5% $\text{HCl} + 5\% \text{HNO}_3 + 90\% \text{C}_2\text{H}_5\text{OH}$	1 min	–	–	–	[82]

a static solution was performed in four different solutions as outlined in Table 4. Among these solutions, using the 50 vol%  $\text{HF} + 50\text{ vol}\% \text{HNO}_3$  solution allowed for the lowest surface roughness value, hence, this solution was chosen for further investigation on the effect of flow and electrolyte composition. It is reported that the  $R_a$  of the 15° build orientation part improved only by 4% (from  $R_a = 7.3\ \mu\text{m}$  to  $R_a = 7.0\ \mu\text{m}$ ) as shown in Figure 13a,b, while, by conducting the CP under solution flow rate of  $10\text{ L min}^{-1}$ , it can be improved up to 23% (from  $R_a = 7.3\ \mu\text{m}$  to  $R_a = 5.6\ \mu\text{m}$ ) as shown in Figure 13c. In this treatment, 50  $\mu\text{m}$  of thickness was removed to achieve the 23% improvement in roughness.<sup>[37]</sup>

Wysocki et al.<sup>[80]</sup> have worked on CP of LB-PBF fabricated titanium alloy scaffolds of different sizes including pores for increased biocompatibility. In their first study, the surface texture of titanium scaffolds was smoothed using  $\text{HF}$  solutions (1–5 vol%) for 1–6 min and using  $\text{HF}$  and  $\text{HNO}_3$  mixtures for 3–9 min. Structures with pore sizes as small as 200  $\mu\text{m}$  were successfully etched with the  $\text{HF}/\text{HNO}_3$  acid mixtures. These results could not be obtained with  $\text{HF}$  acids alone. Based on the mass change and the microscopic observations, the bath composition

was optimized for each scaffold type.<sup>[80]</sup> In another study, Wysocki et al.<sup>[81]</sup> have used CP for post-processing of same scaffolds with some changes in CP parameters. Here, they evaluated three compositions of  $\text{HF}/\text{HNO}_3$  acid mixtures as the polishing medium, and the polishing time for small and large scaffolds were set to 3–9 min and 9–18 min, respectively. Among different solutions that are mentioned in Table 4, the solution containing 1.3 vol%  $\text{HF} + 9.0\text{ vol}\% \text{HNO}_3$  resulted in the highest weight change of the treated parts. This weight loss was reported to be 54%–65% and 27%–38% for the small and large scaffolds, respectively. According to their results, the CP method was effective in removing partially melted powder particles. However, as indicated in Figure 13d, it was not effective when the scaffold has a small pore size and it needs to be adjusted for different scaffold sizes. Hence, further improvement of the proposed polishing process is needed.<sup>[81]</sup> For such complex parts, weight loss measurements are easier to perform than roughness measurements; hence, in this study, the amount of weight loss was used to evaluate the treatment results. However, a recently developed characterization model by Vanderesse et al.<sup>[60]</sup> reports surface roughness characterization based on Micro-CT scanning,

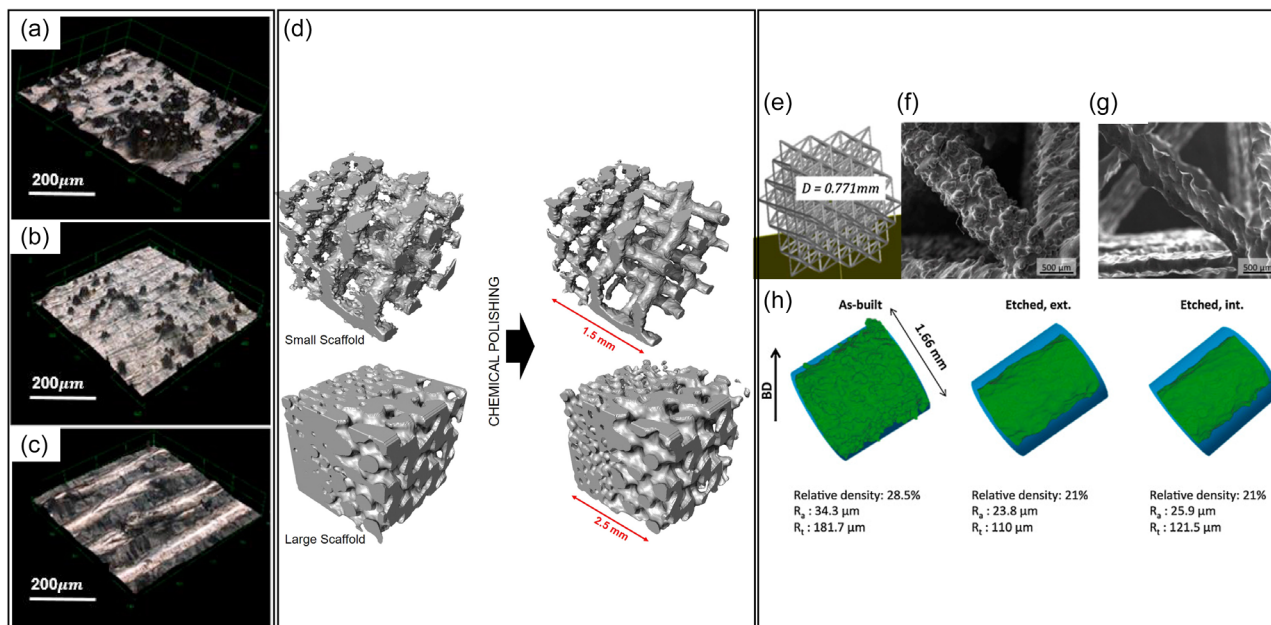


**Figure 13.** Confocal microscope surface image of internal cavity of Inconel part a) As-built condition, after b) static CP, and c) flow CP. Adapted with permission.<sup>[37]</sup> Copyright 2018, Elsevier. d) Micro-CT representative part of the core-shell interface in the small and large scaffold before (left) and after (right) CP. Adapted with permission.<sup>[81]</sup> Copyright 2018, Elsevier. e) CAD model of the octet-truss Ti6Al4V lattice, the SEM image of struts f) in as-built and g) chemical treated condition, and h) the Micro CT scanned representative of strut used for roughness measurement. Adapted with permission.<sup>[83]</sup> Copyright 2016, Elsevier.

which could be applied for these kinds of structures in future studies.

Formanoir et al.<sup>[38]</sup> have performed a chemical etching post-treatment on EB-PBF Ti6Al4V “octet-truss” lattice structures (Figure 13e) by dipping the parts in an aqueous solution containing 3 vol% HF + 13 vol% HNO<sub>3</sub> for 30 min, which was then repeated four times to achieve a favorable surface quality. The morphology changes before and after the chemical treatment was evaluated by SEM as shown in Figure 13f,g. Roughness measurements, for both internal and external struts, computed from the obtained X-ray microtomography data are reported in Figure 13h. According to their results, both internal and external struts had about 27% (from 34.3 to 24.8  $\mu\text{m}$ ) improvement in  $R_a$  roughness value.<sup>[73]</sup>

The use of CP as an effective method to remove the attached feedstock particles was reported by Pyka et al.<sup>[35]</sup> They applied a chemical treatment on LB-PBF produced Ti6Al4V open porous structures containing a significant amount of non-melted powder particles attached to the strut surface throughout the full structure, by immersing the titanium alloy structures in a 0.5 mL HF + 50 g H<sub>2</sub>O solution for 10 min. In this study, the surface roughness improvement for the top part of the strut was about 14% (from  $R_a = 7 \mu\text{m}$  to  $R_a = 6 \mu\text{m}$ ), and it was about 17% (from  $R_a = 12 \mu\text{m}$  to  $R_a = 10 \mu\text{m}$ ) for the bottom struts. The 17% roughness improvement was achieved by 13% (29  $\mu\text{m}$ ) reduction in struth thickness.<sup>[35]</sup>

Wen et al.<sup>[82]</sup> studied the surface quality improvement of pure Zn porous scaffolds printed by LB-PBF using CP. The treatment was performed in a solution consisting of 5% HCl + 5% HNO<sub>3</sub> + 90% C<sub>2</sub>H<sub>5</sub>OH for 60 s. It was observed that after CP,

the spherical particles on the surface were detached, resulting in some volume loss. However, no quantitative analysis regarding mass loss, geometry change, or roughness improvement was reported.

Based on the reviewed paper in this section, we can conclude that CP treatment can significantly improve the quality of internal and external surfaces of AM complex parts. The main disadvantage of this method is the use of strong acids, which is environmentally and operationally hazardous.

## 5. Mechanical Polishing

Mechanical polishing, also known as machining or abrasive finishing, is a conventional post-processing technique to improve surface finishing of any part with accessible surfaces, including those produced by additive manufacturing. This mechanical method is generally described as a controllable material removal process that uses an actuator, and cutting tools or abrasive material to create the intended surface quality.<sup>[15]</sup> Only a few mechanical polishing methods can be used for complex structures. We can categorize them into three groups: 1) abrasive blasting, 2) abrasive flow methods, and 3) hydrodynamic cavitation. Literature related to each group is presented in the following three (Section 5.1–5.3).

### 5.1. Abrasive Blasting

Abrasive blasting, also known as sandblasting (SB), is one of the most commonly used processes for material removal.<sup>[83]</sup> Surface

roughness is influenced by the size, shape, and kinetic energy of the particles. In the SB process, the abrasive particles are accelerated by the air pressure, which increases kinetic energy. The kinetic energy is directly proportional to density, volume, and velocity squared. In Equation (3), kinetic energy is expressed by the parameters introduced. Where  $E_c$  is the kinetic energy,  $V$ ,  $\rho$ , and  $r$  are the velocity, density, and particle radius, respectively.<sup>[84]</sup>

$$E_c = \rho \times \frac{2}{3} \times \pi \times r^3 \times V^2 \quad (3)$$

Teo et al.<sup>[46]</sup> have carried out a study to investigate the influence of SB, as an abrasive post-processing method, on a LB-PBF produced SS 316L lattice structure. SB was performed using a commercially available machine (Peematic 750S, Swiss Instruments Limited, Mississauga, ON, Canada) with a nozzle diameter of 5 mm. A distance of 100–120 mm was maintained between the sample and the workpiece, pressures ranging from 60 to 80 psi were applied, and glass beads ( $B_2O_3$ ,  $B_4C$ ,  $BiO_3$ ,  $CaO$ ) with diameters of 200–300  $\mu m$  were employed. Using SB, the partially melted particles were effectively removed (compare **Figure 14a,b**). However, the surface has been damaged, introducing a peel-off layer (**Figure 14c**) and leaving residue on the treated surface (**Figure 14d**). As-built roughness values were evaluated as  $S_a = 15 \mu m$  and  $S_z = 55 \mu m$ , which were then reduced by 67% (to  $S_a = 5 \mu m$ ) and 32% (to  $S_z = 37 \mu m$ ), respectively, after one SB step. However, no information was document about the thickness change.<sup>[46]</sup>

In another study by Ahmadi et al.<sup>[85]</sup> SB was used to eliminate surface imperfections of a LB-PBF fabricated Ti6Al4V lattice structure. SB was performed during 150 s using  $Al_2O_3$  abrasive particles with particles size ranging from 180 to 220  $\mu m$ . It was confirmed that SB could not penetrate to the core of the lattice structure and it could only treat the external struts, as can be witnessed in **Figure 14e**. The strut thickness reduction and

sample weight loss after SB were reported as  $20.5 \pm 4.5\%$  and  $5.5 \pm 1.3\%$ , respectively.<sup>[85]</sup>

Another study on the use of SB to improve LB-PBF produced Ti6Al4V lattice structure surface roughness was documented by Karami et al.<sup>[24]</sup> They conducted the SB deploying abrasive  $Al_2O_3$  particles (50  $\mu m$  diameter) for 90 s with a nozzle pressure of 4.5 bar and a sample rotation speed of 200 rpm. The results of roughness measurements were not reported, but their SEM analysis shown in **Figure 15a** indicates that SB is only effective for the external struts and cannot penetrate deeply into the lattice structure,<sup>[24]</sup> as confirmed by Ahmadi et al.<sup>[85]</sup>

Wen et al.<sup>[82]</sup> employed SB to enhance the surface quality of pure Zn porous scaffolds produced by LB-PBF. SB utilized spherical glass beads with a diameter of 100–200  $\mu m$  at a pressure of 2.5 MPa. The SEM micrographs of the scaffolds before and after SB are depicted in **Figure 15b** at two different magnifications. It was observed that the majority of attached particles were either removed or flattened due to the impact of blasted glass beads. However, several holes remained due to the varied sizes and random distribution of attached particles. They concluded that achieving uniform surface quality via SB, especially for porous scaffolds with numerous corners and cavities, posed challenges. Additionally, they found that the applicability of SB for such complex parts was limited. Therefore, they suggested considering other post-processing methods for further improvement. Similar to their study on CP within the same publication, detailed information about the SB process and quantitative measurements of roughness and thickness variation were not provided.<sup>[82]</sup>

According to the reviewed paper in this section, we can highlight that SB improve surface quality on a macroscopic scale and is known as one of the most cost and time efficient post-processing techniques. However, it may cause some microscopic defects such as peel-off layers and residual particles. Moreover, according to the SEM images provided in the literature, it cannot influence the internal struts in the core of lattice structures.

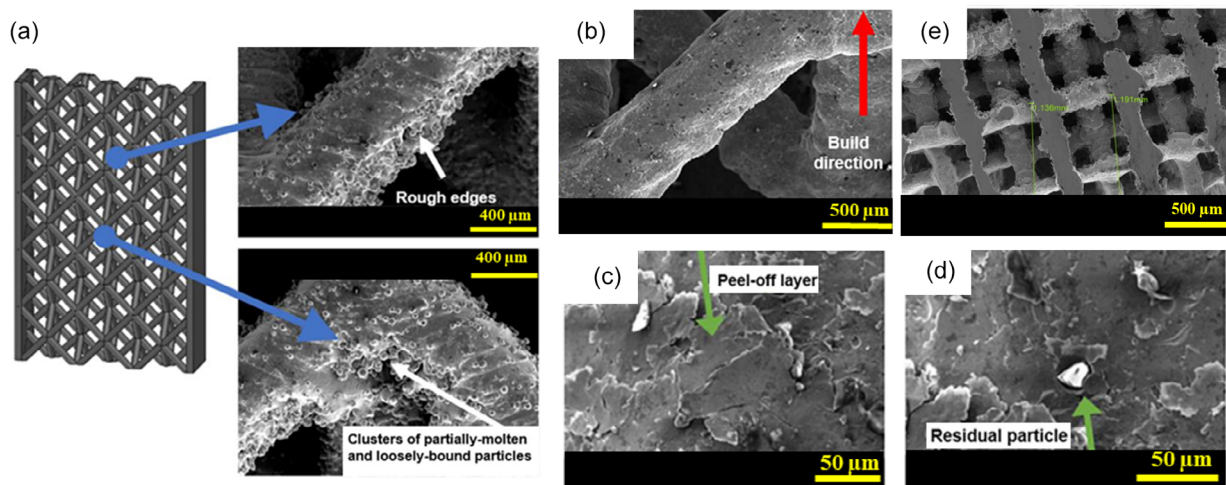


**Figure 14.** SEM images of 316L lattice structure in a) as-printed and b) sand-blasted, with defects c) peel-off layer and d) residual particles. Adapted under the terms of the CC BY 3.0 license.<sup>[46]</sup> Copyright 2021, The Authors. Published by MDPI. e) SEM image of lattice structure after CP. Adapted with permission.<sup>[85]</sup> Copyright 2018, Elsevier.



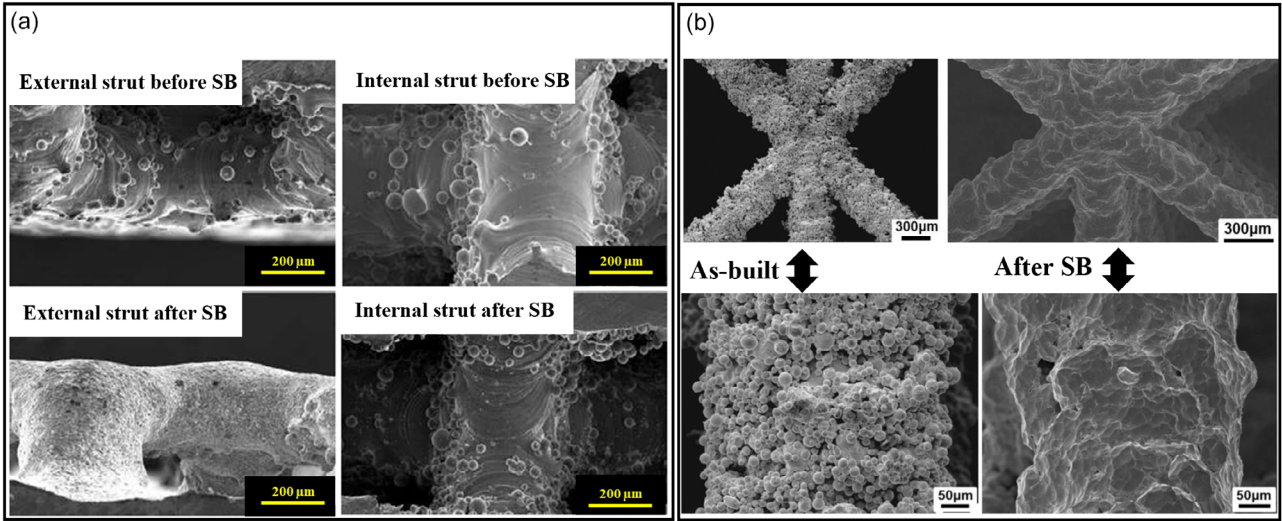


**Figure 15.** a) SEM images of internal and external struts before and after SB of Ti6Al4V. Adapted under the the terms of the CC BY 4.0.<sup>[24]</sup> Copyright 2020, The Authors. Published by Elsevier. b) SEM images of Zn porous scaffold in as-built condition and after SB at different magnifications. Adapted with permission.<sup>[82]</sup> Copyright 2018, Elsevier.

## 5.2. Abrasive Flow Methods

In this section, two different methods of abrasive flow machining (AFM) and abrasive flow polishing (AFP) are discussed. AFM is a non-conventional finishing procedure that involves a “semi-solid medium” consisting of a viscoelastic polymer and abrasive particles mixed in a definite ratio. To achieve the desired surface quality, this media is extruded under pressure through or across the surface.<sup>[86]</sup> There are three modes of material removal by AFM: elastic deformation, plastic deformation, and micro-cutting. Deformation modes in abrasives are strongly dependent on the magnitude of cutting forces acting on individual grains of abrasive and the depth of the indentation produced by those grains in the workpiece.<sup>[87,88]</sup> The AFP process involves the flow

of pressurized “slurry” in turbulent mode over the surface. The abrasive slurry must have a velocity and kinematic viscosity such that the Reynolds number exceeds the critical value of 2300 in order to remain turbulently suspended.<sup>[89]</sup> Hence, it is the viscosity of the polishing medium that is the major difference between AFM and AFP. AFM employs a viscous polymer, while AFP uses a fluid medium as the base for abrasive particles.

Mohammadian et al.<sup>[37]</sup> used AFM (schematic is shown in **Figure 16a**) to improve surface quality of LB-PBF components made of Inconel 625. As an abrasive, Kramer Industries aluminum oxide grit with an average particle size of  $d_{45} = 420 \mu\text{m}$  and specific gravity of 3.94 was used. Further AFP parameters including the abrasive particle concentration in water (base fluid), the volume of polishing media, and the flow rate were 6 wt%, 5 L,

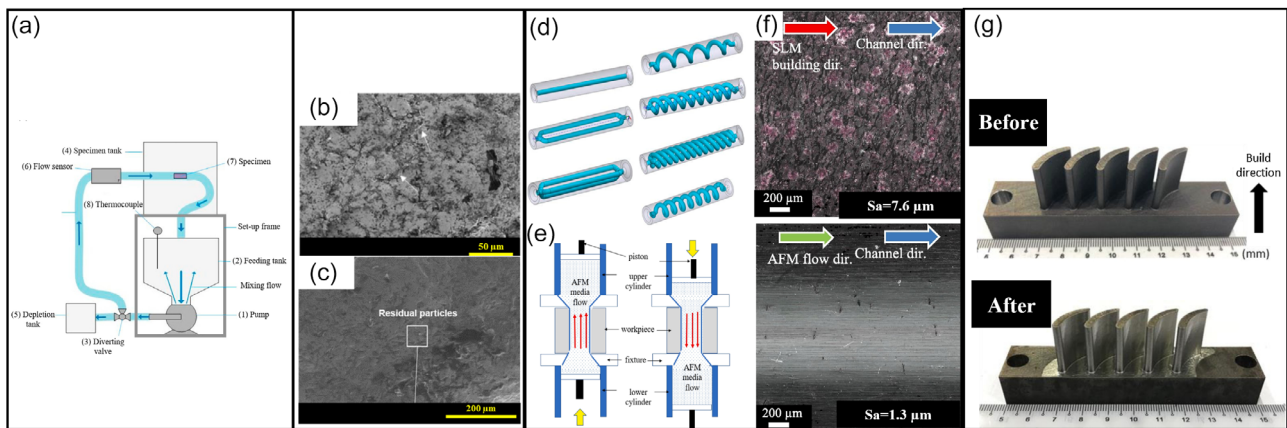


**Figure 16.** a) Schematic of AFM apparatus. Adapted with permission.<sup>[37]</sup> Copyright 2017, Elsevier. b) Focus variation microscopy of surface, arrows indicating areas of peel-off layer removal/smoothing, c) residual particles after AFM. Adapted under the the terms of the CC BY 3.0.<sup>[46]</sup> Copyright 2021, The Authors. Published by MDPI. d) seven types of conformal cooling channels ( $\varnothing$ 3 mm), e) A schematic illustration of a two-way AFM, f) Optical micrographs of single straight channels before and after AFM. Adapted with permission.<sup>[47]</sup> Copyright 2020, Elsevier. g) Nozzle guide vane blades before and after AFM. Adapted with permission.<sup>[39]</sup> Copyright 2020, Elsevier.

and 10 L min<sup>-1</sup>, respectively. The pumping pressure was 32.2 psi and polishing times of 1, 2, and 3 h were considered. Deploying AFP for 1 h on the Inconel AM parts in these process conditions, resulted in a 18% surface roughness improvement (from  $R_a = 7.3 \mu\text{m}$  down to  $R_a = 6.0 \mu\text{m}$ ), which could be increased to around 30% (from  $R_a = 7.3 \mu\text{m}$  down to  $R_a \approx 5 \mu\text{m}$ ) by further polishing of 3 h.<sup>[37]</sup>

Teo et al.<sup>[46]</sup> used AFP after SB of LB-PBF SS316 lattice structures. SiC, Al<sub>2</sub>O<sub>3</sub>, B<sub>4</sub>C, and steel grit with 3%, 4%, 3%, and 90% weight percentage were used as abrasive particles. The sizes of SiC, Al<sub>2</sub>O<sub>3</sub>, B<sub>4</sub>C were below 10  $\mu\text{m}$  whereas the average steel grit was 150  $\mu\text{m}$ . The AFP setup was equipped with a pneumatic piston with a fixed vibration frequency of 30 Hz. Based on observed microstructures in Figure 14b and 16b, it was determined that SB caused peel-off layers that were removed by abrasive polishing. According to the measurements, AFP was not found to be effective in improving surface roughness values after SB. This experiment did not alter the  $S_a$  roughness parameter ( $S_a = 5 \mu\text{m}$ ). Furthermore, the measured  $S_z$  value was 53  $\mu\text{m}$ , which was comparable with the as-printed condition. This indicates that abrasive polishing may introduced surface pits, causing the  $S_z$  to increase. Moreover, residual particles with diameters between 2 and 5  $\mu\text{m}$  were observed in Figure 16c.<sup>[46]</sup>

Han et al.<sup>[47]</sup> used AFM to improve surface finishing of conformal cooling channels created by LB-PBF. As shown in Figure 16d, conformal cooling channel geometries comprise a mixture of single/multiple and straight/helical channels, which create different lengths to diameter ratios between 40 and 240. In this study, a total of seven different types of conformal cooling channels ( $\phi 3 \text{ mm}$ ) made of Maraging steel 300 were used. After the part was clamped into the AFM fixture, the internal channels were polished by flowing AFM media, ULV50%-54 (mixture of polymers and SiC), through them for ten cycles, at the extrusion pressure of 80 bars. In the two-way AFM machine shown in Figure 16e, a cycle is completed by full movement of the up and down strokes. After cutting the parts, focus variation microscopy was used to determine the surface topography of internal channels of seven types. In comparison with as-built surfaces, AFM improved all cooling channel surface roughness parameters, however, it was the geometry that determined the amount of improvement. In the part with a single straight channel, the surface roughness was reduced by 82% from  $S_a \approx 7.6 \mu\text{m}$  to  $S_a \approx 1.3 \mu\text{m}$  (Figure 16f). The lowest improvement was seen in the three helical channels, in which  $S_a$  roughness was reduced by 43% (from  $S_a \approx 9.6 \mu\text{m}$  to  $S_a \approx 4.5 \mu\text{m}$ ).<sup>[47]</sup>

Freeform surfaces produced via additive manufacturing can also be improved by AFM. Accordingly, Kum et al.<sup>[39]</sup> deployed AFM experiments on nozzle guide vane blades, which are shown in Figure 16g. The part produced by an LB-PBF machine and was made of Maraging steel MS1. An industrial AFM equipment from Extrude Hone Corporation, the EX4250, was used for the AFM experiments. Commercial AFM media AMV36, which is medium viscosity and is fielded with silicon carbide abrasive particles of grit size 700  $\mu\text{m}$ , was used. Initially, the blades had a surface roughness in the range of 5–15  $\mu\text{m}$ , which was reduced by AFM to a roughness of less than 1  $\mu\text{m}$ . This study shows that achieving good surface roughness during the AFM process is not a challenge, however, uneven material removal can have an impact on the final accuracy of the polished part. Depending

on the profile of the blade, material removal ranged from 50 to 550  $\mu\text{m}$ .<sup>[39]</sup>

According to the reviewed papers in this section, we can conclude that the use of abrasive methods will result in a surface quality improvement of 0% to 90%. The treatment performance is highly dependent on part geometry and process parameters. Furthermore, the process is slow and it will not remove material evenly, which can lead to problems with part geometry accuracy on complex parts.

### 5.3. Hydrodynamic Cavitation

The use of AFM to process AM-fabricated internal channels may be promising, but the material removal rate (MMR) is slow, resulting in a long processing time.<sup>[42]</sup> In complex AM parts, AFM may cause an agglomeration of abrasive material. A further increase in pumping pressure could damage the thin walls of the channel.<sup>[41]</sup> Hydraulic cavitation abrasive finishing (HCAF, the schematic is shown in Figure 17a) was recently developed to address the problems of agglomeration and excessive thickness loss during surface finishing. One of the major erosion categories identified in fluids is cavitation. Cavitation occurs when a fluid's hydrostatic pressure reaches the vapor pressure at a given temperature in a hydrodynamic flow. Cavitation and the presence of solid particles in a hydrodynamic flow are thought to be destructive. In contrast, the bubble-particle interaction generated by cavitation is highly effective for finishing internal surfaces. In AM complex internal channels, controlled cavitation associated with sharp-edged micro-abrasives removes surface irregularities.<sup>[40,41]</sup>

Nagalingam and Yeo<sup>[41]</sup> proposed an innovative method to finish the internal surfaces of AlSi10Mg LB-PBF circular channels using hydrodynamic flow at cavitation conditions and free-floating abrasives. HCAF was performed at a velocity of 34 m s<sup>-1</sup>, an absolute downstream pressure of 13.325 kPa, and cavitation number of 0.0065, with four level of abrasive concentrations of 0, 1, 5, and 10 wt% for 5 h. Hard-cut silica particles with a diameter of about 10  $\mu\text{m}$  were used as abrasives, and water was used as a working fluid at a temperature of 45 °C.  $S_a$  surface roughness value was decreased by 40% (from  $S_a = 49.8 \mu\text{m}$  to  $S_a = 29.7 \mu\text{m}$ ) in their experiment containing 10% abrasive particles, while the experiment with no abrasive particles showed only 17% (from  $S_a = 46.3 \mu\text{m}$  to  $S_a = 38.4 \mu\text{m}$ ) reduction in surface roughness.<sup>[41]</sup>

To investigate the synergistic effect of HCAF, Nagalingam et al.<sup>[42]</sup> performed four comparative experiments to treat internal surfaces of AlSi10Mg square-shape channels produced by LB-PBF. The four experiments in this study were designed based on the individual phenomenon that contribute in HCAF. Hence, the experiments in the study were performed during 150 min as follows: 1) liquid impingement; 2) pure cavitation; 3) pure abrasion; and 4) HACF. During first treatment under liquid impingement condition, three different temperatures of 45, 50, and 55 °C were considered, which improved surface roughness by -10.9%, -5.5%, and 1%, respectively. The negative improvement can be attributed to the fact that liquid impingement can only remove loosely attached powder. If only loose particles are removed, the asperities beneath the loose



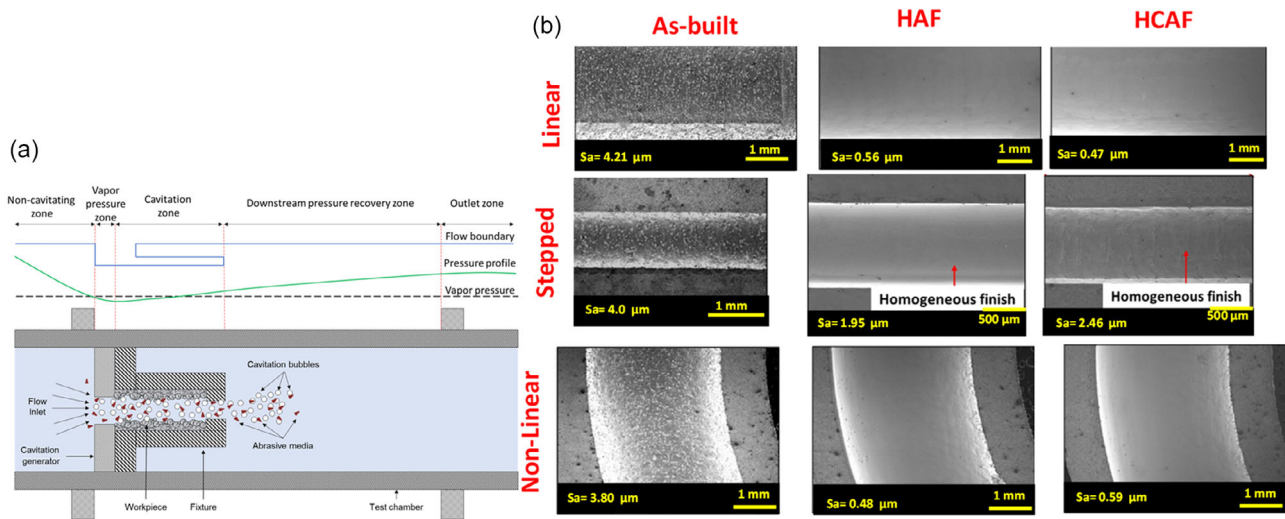


**Figure 17.** a) Material removal mechanism in HCAF. Adapted with permissions.<sup>[41]</sup> Copyright 2020, Elsevier. b) Surface morphology of the best samples in each category of channels in as-built format, after HAF and after HCAF. Adapted with permission.<sup>[40]</sup> Copyright 2020, Elsevier.

particles are exposed, resulting in sharper peaks and increased  $R_a$  values. Second treatment, pure cavitation, was performed in three different temperatures of 45, 50, 55 °C and two upstream pressures of 0.35 and 0.7 MPa. Only the treatment at  $T = 50$  °C and  $P_u = 0.7$  MPa improved  $R_a$  roughness value by 6.5%. All other temperatures and upstream combinations had negative or no effect on surface quality. In this experiment, the effective bubble collapse was achieved at  $T = 50$  °C and  $P_u = 0.7$  Mpa, which removed loosely attached and partially melted particles and slightly improved surface quality. In the next treatment which was performed under pure abrasion, three different temperatures of 45, 50 and 55 °C and two different abrasive concentration of 0.5% and 1.0% were considered. All experiments resulted in positive surface roughness improvement in the range of 10.5% (at  $T = 45$  °C,  $A_c = 0.5\%$ ) to 14.3% (at  $T = 55$  °C and  $A_c = 1.0\%$ ). The improvement in surface quality increased with increase in temperature and abrasive particle concentration. Finally, in HCAF treatment, three temperatures of 45, 50, 55 °C; two upstream pressures of 0.35 and 0.7 MPa; and two abrasive concentrations of 0.5% and 1.0% were selected to investigate the synergistic effect. The lowest roughness improvement was reported as 10.22% which was obtained after HCAF at  $T = 45$  °C,  $P_u = 0.35$  Mpa and  $A_c = 0.5\%$ . On the other hands, the highest improvement of 91.45% was obtained while treatment at  $T = 50$  °C,  $P_u = 0.7$  MPa and  $A_c = 1.0\%$ . As a result, in HCAF conditions the synergistic effect resulted in surface finish enhancement of over 90% ( $R_a$ ) and material removal rate of 80% above those obtained from pure cavitation and abrasion. The thickness decreased only 0.7 μm, which was equivalent to a 0.035% reduction compared to the as-built thickness.<sup>[42]</sup>

The authors<sup>[40]</sup> have conducted a novel study on surface finishing of complex internal channels of LB-PBF Inconel 625. The study investigates hydrodynamic finishing of linear, stepped, and non-linear internal channels with diameters of 1–5 mm and lengths up to 100 mm by a multi-jet hydrodynamic cavitation abrasive finishing apparatus (MJ-HCAF). The MJ-HCAF machine was an upgraded version of the HCAF machine since

it has two types of pressure cavitation-injection pressure ( $P_{u1}$ ) and slurry-injection pressure ( $P_{u2}$ ). Using this new system, two different finishing experiments were used in this study, 1) hydrodynamic abrasive finishing (HAF) in which the internal channels were finished by pure slurry flow, and 2) hydrodynamic cavitation abrasive finishing (HCAF) in which combination of cavitation and slurry loops were used to internal surface finishing. As a result, the surface texture was uniform within linear and non-linear internal channels. To achieve a uniform surface finish, step-like channels can be replaced with gradually tapered channels. In general, the hydrodynamic finishing technique improve the surface quality depending on the geometry of the channel. The best improvements were achieved by HAF in some experiments and by HCAF in others. Figure 17b shows the surface morphology of samples having the most improvement in each channel type, in as-built format, after HAF and HCAF. According to the results for linear channels, HCAF reduced  $S_a$  roughness by 89% from 4.21 to 0.47 μm. In curved non-linear channels, HCAF resulted in an 87% reduction of  $S_a$  roughness from 3.80 to 0.48 μm. In contrast, HAF worked better for the stepped channel, which can reduce its roughness by 51% (from  $S_a = 4.0$  μm to  $S_a = 1.95$  μm).<sup>[40]</sup>

According to the reviewed literature in this section, we can highlight that hydrodynamic cavitation methods can effectively improve surface quality of AM parts and by manipulating the process parameters higher surface roughness improvements can be achieved faster. Additionally, it requires less pressure than AFM, making it an ideal candidate for surface treatment of delicate AM parts. Table 5 summarizes the mechanical treatments that were studied, along with their corresponding experimental conditions and the resulting enhancements in roughness.

## 6. Hybrid Methods

Several research studies have examined the effects of combining treatments on AM parts to maximize their synergistic effect.

**Table 5.** Summary of mechanical polishing and their performance for AM complex parts.

Material	Mechanical method	Other conditions	Time	Max Roughness improvement (roughness values are in $\mu\text{m}$ )	Thickness reduction (relative and absolute)	References
SS316 (lattice)	SB	Nozzle diameter = 5 mm, distance = 100–120 mm, pressures = 60–80 psi, and glass beads' size = 200–300 $\mu\text{m}$	NA	66% ( $S_a$ : 15 to 5)	–	[46]
Ti6Al4V (lattice)	SB	$\text{Al}_2\text{O}_3$ particle size = 180–200 $\mu\text{m}$	150 s	–	20.5%	[85]
Ti6Al4V (lattice)	SB	Nozzle pressure = 4.5 bar, rotation speed 200 RPM, $\text{Al}_2\text{O}_3$ particle size = 50 $\mu\text{m}$	90 s	–	–	[24]
Inconel 625 (Internal cavity)	AFP	$\text{Al}_2\text{O}_3$ particle size = 420 $\mu\text{m}$ , specific gravity = 3.94, fluid = water, concentration = 6 wt%, volume of polishing media = 5 L, flow rate = 10 L $\text{min}^{-1}$ , Pumping pressure = 32.2 psi	1,2,3 h	30% ( $R_a$ : from 7.3 to 5)	–	[37]
SS316 (lattice)	AFP	Abrasive slurry = 3% SiC ( $\leq 10 \mu\text{m}$ ), 4% $\text{Al}_2\text{O}_3$ ( $\leq 10 \mu\text{m}$ ), 3% $\text{B}_4\text{C}$ ( $\leq 10 \mu\text{m}$ ) and 90% steel grit (150 $\mu\text{m}$ )	NA	0% ( $S_a = 5$ )	–	[46]
Marging steel 300 (internal hole)	AFM	Abrasive media = MV50%–150, Flow volume per one cycle = 0.66 L, pressure = 80 bar, number of cycles = 10	NA	82% ( $S_a$ : from 7.6 to 1.3)	–	[47]
Marging steel MS1 (free form surface)	AFM	Abrasive media = MV36, particle grit size = 700 $\mu\text{m}$ , Pressure = 10 Mpa, number of cycles = 6,	NA	93% ( $R_a$ : from 15 to 1)	$0 \approx 325 \mu\text{m}$	[39]
AlSi10Mg (internal hole)	HCAF	Abrasive media = water + SiC (0, 1, 5, 10 wt%), SiC particle size = 10 $\mu\text{m}$ $T = 45^\circ\text{C}$ , pressure = 13.325 kPa, cavitation number = 0.0065, velocity = 34 $\text{m s}^{-1}$	5 h	40% ( $S_a$ : from 49.8 to 29.7)	–	[41]
AlSi10Mg (internal hole)	HCAF	$P_u = 0.7 \text{ MPa}$ ; $P_d = 0.1 \text{ MPa}$ ; $T = 50^\circ\text{C}$ ; $A_c = 1.0\%$	150 min	91% ( $R_a$ : from 20 to 2)	0.035%, 0.7 $\mu\text{m}$	[42]
Inconel 625 (internal hole)	Multi-jet HCAF	Abrasive media = water + SiC ( $\leq$ ), SiC particle size = 30 $\mu\text{m}$ $T = 25^\circ\text{C}$ , Pressure = 0.1 Mpa, slurry pressure = 1.5 Mpa	15 min	Linear channel: 89% ( $S_a$ : from 4.21 to 0.47) Stepped channel: 51% ( $S_a$ : from 4.0 to 1.95) Non-linear Channel: 87% ( $S_a$ : from 3.80 to 0.48)	– – –	[40]
Pure Zn	SB	Glass bead particle size = 100–200 $\mu\text{m}$ , $P = 2.5 \text{ MPa}$	NA	NA	–	[82]

In this section, three combinations of chemical-electrochemical, mechanical-electrochemical, and mechanical-chemical are discussed.

### 6.1. Combination of CP and ECP

As elaborated in section 4 CP method does not rely on electrodes or their positioning such as ECP does.<sup>[90]</sup> Hence, CP and ECP can be combined to take advantage of each method. Dong et al.<sup>[21]</sup> have proved that CP can be applied in advance to help ECP go deeper inside the Ti6Al4V lattice part manufactured by LB-PBF. In this study, an aqueous solution containing 1% HF

and 20%  $\text{HNO}_3$  was used for CP and another solution combination of 995 mL ethanol, 100 mL n-butyl alcohol, 109 g of  $\text{Al}(\text{H}_2\text{O})_6\text{Cl}_3$ , and 250 g  $\text{ZnCl}_2$  was used for ECP. A DOE was used to study the synergistic effect of CP and ECP treatments. Profilometer roughness measurement of internal struts showed no improvement on samples without CP. On the other hand, with the combination of chemical and ECP, roughness improvement was up to 46%, with  $3 \approx 4\%$  ( $75 \approx 100 \mu\text{m}$ ) strut thickness reduction. **Figure 18a** shows that pre-treatment with CP can improve internal surface roughness, whereas experiments with only ECP had no influence on internal surfaces. In **Figure 18b** the optical images of the internal surface profile of lattice

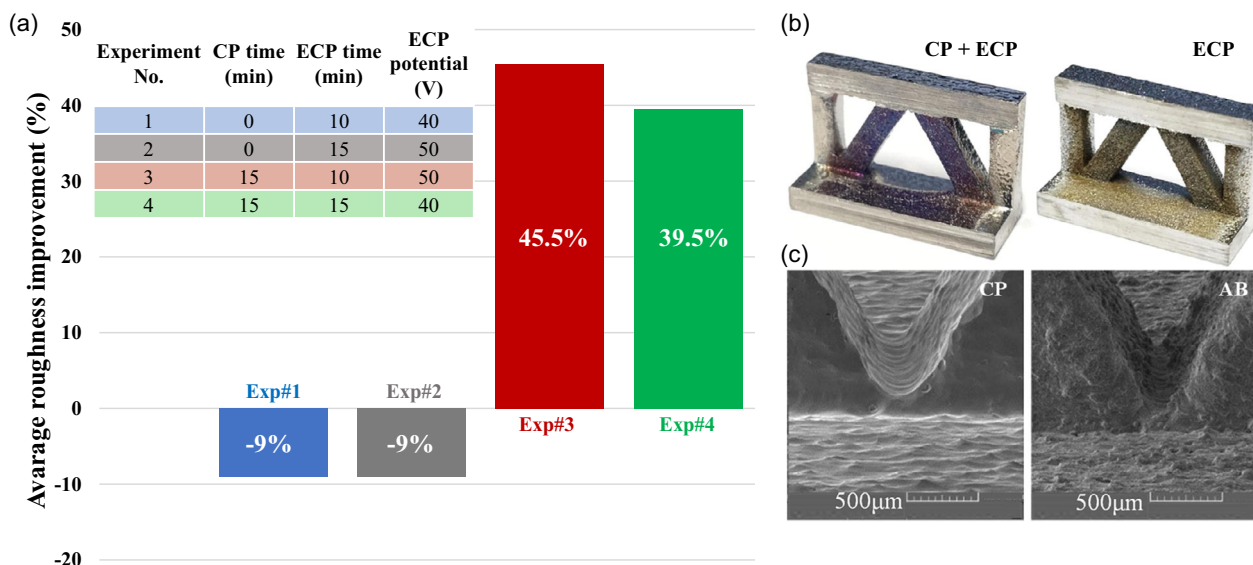


**Figure 18.** a) DOE table for the treatment experiment of Ti6Al4V lattice structure and surface roughness measurement results b) Optical image after combination CP and ECP (left) and only ECP (right). c) SEM image of the internal surface after CP (left) and in as-built condition (right). Adapted with permission.<sup>[21]</sup> Copyright 2019, Springer.

structures, one after 15 min CP and 15 min ECP and the other after only 15 min of ECP, are shown. The ECP potential in both experiments was 50 V versus SS cathode material, and other processing conditions for these two parts were exactly the same. It can be concluded from these optical images that the internal surface of the part after ECP is nearly intact. On the other hand, Figure 18c compares SEM images of chemical polished and as-built part and it shows how the texture of internal surfaces can vary after one step of CP.<sup>[21]</sup>

In another study, Pyka et al.<sup>[35]</sup> have used a combination of CP and ECP for surface modification of Ti6Al4V cylindrical porous structure which was produced by LB-PBF. In this research both CP and ECP were HF based with composition of 0.5 vol% HF + 50 g H<sub>2</sub>O and 15 mL HF + 55 mL CH<sub>3</sub>COOH + 30 mL H<sub>2</sub>SO<sub>4</sub>, respectively. Hybrid chemical and ECP was applied to two different as-built parts. The CP treatment was performed for 10 min for both parts and ECP was performed for 6 min for one part and 8 min for the other. The results of individual ECP and CP treatment in this study were presented in Section 3 and 4. In **Figure 19a**, the surface roughness values and roughness reductions of top struts and bottom struts, in as-produced condition, and after CP, ECP, and two CP + ECP experiments are compared. According to the authors, by using this protocol, AM Ti6Al4V open porous structures can achieve significant and controllable roughness reduction. The most significant improvement in roughness was 50%, achieved through a reduction in thickness of 50 µm (22%). CP removed the attached powder particles, whereas ECP further reduced surface roughness. By doing so, the heterogeneity of the strut surface roughness was effectively improved throughout the entire 3D structure. This fact became more obvious by referring to the SEM image of the struts in different conditions of as-built, after CP, and after hybrid ECP and CP that is shown in **Figure 19b**.<sup>[35]</sup>

Langi et al.<sup>[44]</sup> used a combination of CP and ECP to improve the surface quality of SS 316L stents produced by LB-PBF. The CP involved immersing the part in an aqueous acid solution containing 3 mL HF + 9 mL HNO<sub>3</sub> + 88 mL H<sub>2</sub>O at 25 °C for 3 min. The CP treatment was followed by ECP in electrolyte consisting of 42 mL H<sub>3</sub>PO<sub>4</sub> + 47 mL C<sub>3</sub>H<sub>8</sub>O<sub>3</sub> + 11 mL H<sub>2</sub>O. During ECP, the temperature was maintained at 75 °C, and the applied potential and current were 12 V and 1.2 A, respectively. The ECP lasted for 1.5 min, divided into three 30-second steps. This hybrid treatment resulted in a 29% improvement in roughness by reducing  $R_a$  from 8.45 to 5.96 µm. The mass reduction for each treatment was documented separately. CP caused a mass loss of 487.80 mg, which accounted for 2.1% of the as-built mass. ECP caused a mass loss of 487.40 mg, i.e., representing 1.9% of the mass of the stent after CP. Despite the reported roughness improvement and mass loss of the stent, microscopic studies depicted in **Figure 20a** reveal that many partially melted particles remain attached to the surface, and the strut uniformity is significantly inferior to that of commercial stents produced by laser micromachining.<sup>[44]</sup>

Wen et al.<sup>[82]</sup> investigated the combined effect of CP and ECP on the roughness improvement of pure Zn scaffolds produced by LPBF. The treatment consisted of two steps. In the first step, CP was performed using a solution mixture of 5% HCl + 5% HNO<sub>3</sub> + 90% C<sub>2</sub>H<sub>5</sub>OH for 20 s. The second step involved ECP in a solution comprising 50% H<sub>3</sub>PO<sub>4</sub> + 50% C<sub>2</sub>H<sub>5</sub>OH for 10 min, with a current density of 2.25 A m<sup>-2</sup> provided by a potential of 16 V. Strut thickness measurement was conducted to observe the amount of material removed during this process, and it was documented that the diameter of struts reduced from 300 to 250 µm. **Figure 20b** shows the SEM micrographs of the scaffold in as-built condition, after CP and after CP + ECP. It could be observed that after

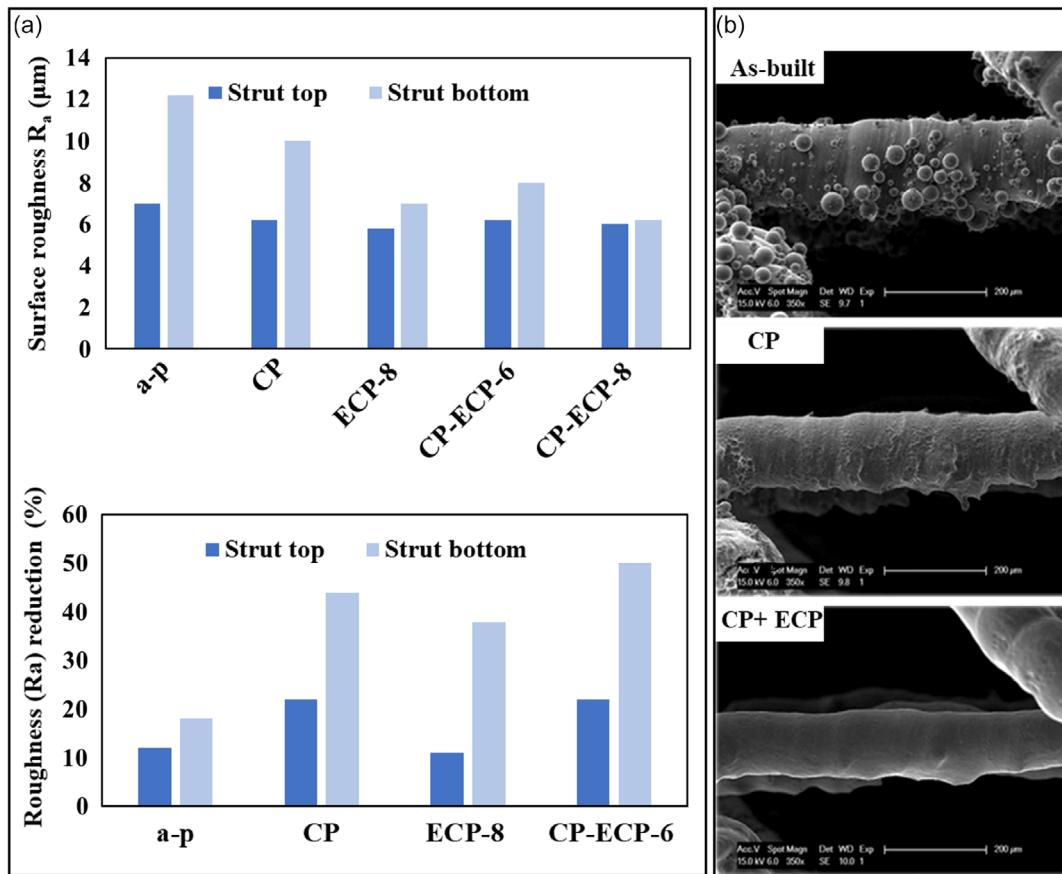


**Figure 19.** a) surface roughness and its reduction in different post-processing conditions of Ti6Al4V cylindrical lattice b) SEM images in different conditions of as-built, after CP and after combination of CP and ECP. Reproduced and Adapted with permission.<sup>[35]</sup> Copyright 2012, Wiley.

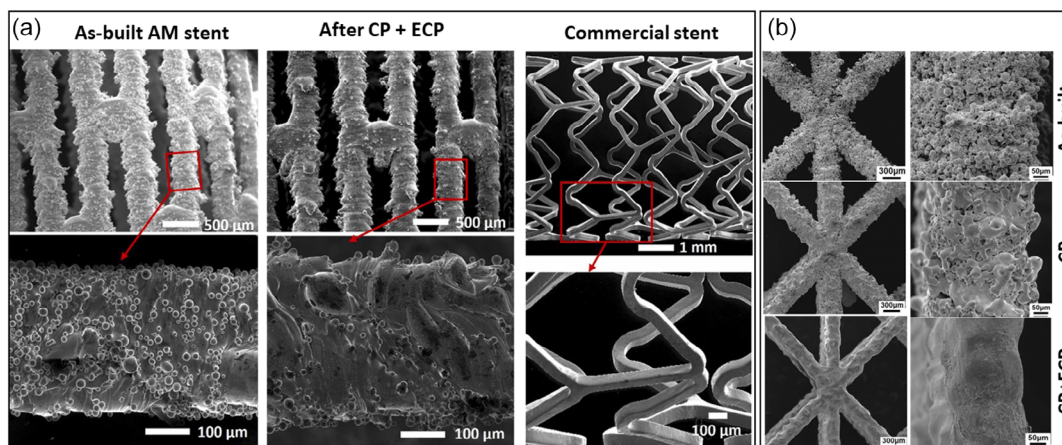


**Figure 20.** a) SEM images of stent at various magnifications in its as-built condition (left), after CP (middle), and after CP + ECP. Adapted with permissions.<sup>[44]</sup> Copyright 2022, Elsevier. b) SEM images of Zn porous scaffold in as-built condition, after CP, and after CP + ECP. Adapted with permissions.<sup>[82]</sup> Copyright 2018, Elsevier.

60 s of CP, the smaller partially melted particles at the surface were removed, while the larger ones remained, resulting in a texture that was not very smooth with CP alone. However, a significant improvement was observed with

the hybrid treatment of 20 s CP followed by 10 min of ECP. With this combined treatment, all attached particles disappeared, and the diameter of the struts became uniformly reduced.<sup>[82]</sup>



According to these studies which combine CP and ECP, we can highlight that this approach will 1) take the roughness improvement deep to the lattice structure, and 2) can result in a smoother surface compared to individual treatments.

## 6.2. Combination of Mechanical and Electrochemical

A combination of cavitation peening and ECP was used by Wang et al.<sup>[48]</sup> to improve the surface roughness of a SS316 AM lattice part produced by LB-PBF. In this study, two types of experiments were performed. The first experiment was a “sequential process” containing 10 min of ECP followed by 10 min of cavitation peening. The second experiment was the “hybrid process,” in which both ECP and cavitation peening were conducted simultaneously for 10 min. In order to accomplish this, an experimental setup (Figure 21a), where cavitation peening and ECP are performed simultaneously, was utilized. An environmentally friendly sulfuric acid-free electrolyte was used in the ECP process, with the mixture of 42 wt% H<sub>3</sub>PO<sub>4</sub> (with purity of 85 wt%), 47 wt% glycerol, and 11 wt% DI. ECP was performed under the potential of 16 V and current of 2 A, in a two-electrode system in which ultrasonic horn (or cavitation nozzle) acted as the cathode material and the workpiece was the anode. Cavitation peening was performed using a high-power ultrasonic sonifier (Branson SFX 550) in a continuous mode under frequency of 20 kHz with two different amplitudes of 56 μm and 84 μm and the distance of 5 mm from the workpiece. In terms of improving the surface roughness, both processes improved the roughness to nearly the same extent. This improvement was approximately 58% for sequential processes (from  $S_a = 9.952 \mu\text{m}$  to  $S_a = 4.122 \mu\text{m}$ ) and about 64% for hybrid process (from  $S_a = 9.952 \mu\text{m}$  to  $S_a = 3.579 \mu\text{m}$ ). The hybrid process has an advantage over the

sequential in terms of improvement rate, since this improvement was achieved in 10 min, whereas it took 20 min for sequential. Figure 21b shows SEM images of the lattice struts before and after postprocessing. The particles adhered to the as-built surfaces were removed effectively, resulting in smoother surfaces. Surface dimples are also visible as a result of cavitation peening. According to the authors, however, the hybrid process was only able to effectively treat the top one or two layers of the lattice structures in these experiments. To treat the entire lattice structure in one step, the parameters of the ultrasonic horn, such as the vibration amplitude and frequency, need to be further optimized.<sup>[48]</sup>

Teo et al.<sup>[46]</sup> used two different routines for combination of mechanical and ECP for post-processing of SS316L lattice structures produced by the LB-PBF method. One routine involves SB and ECP, and the other involves SB, abrasive polishing, and ECP. SB was performed using Peenmatic 750S machine with a nozzle diameter of 5 mm, the working distance of 100–120 mm, pressure range of 60–80 psi, and glass bead diameter of 200–300 μm. In abrasive polishing SiC, Al<sub>2</sub>O<sub>3</sub>, B<sub>4</sub>C and steel grit with an amount of 3 wt%, 4 wt%, 3 wt% and 90 wt%, respectively, were used as abrasive particles. The sizes of SiC, Al<sub>2</sub>O<sub>3</sub>, B<sub>4</sub>C were below 10 μm, whereas the average steel grit was 150 μm. The abrasive polishing setup was equipped with a pneumatic piston with a fixed vibration frequency of 30 Hz. ECP carried out using commercially available setup according to ASTM A380 standard for surgically implantable SS devices. An electrolyte with mixture of 90 vol% H<sub>3</sub>PO<sub>4</sub> and H<sub>2</sub>SO<sub>4</sub> at temperature of 45–50 °C was used in ECP of the part for 10–30 min. After post-processing of lattice structure by first routine, the  $S_a$  surface roughness has changed from 15 to 3 μm which is an 80% improvement in surface quality. In the second routine, the surface roughness

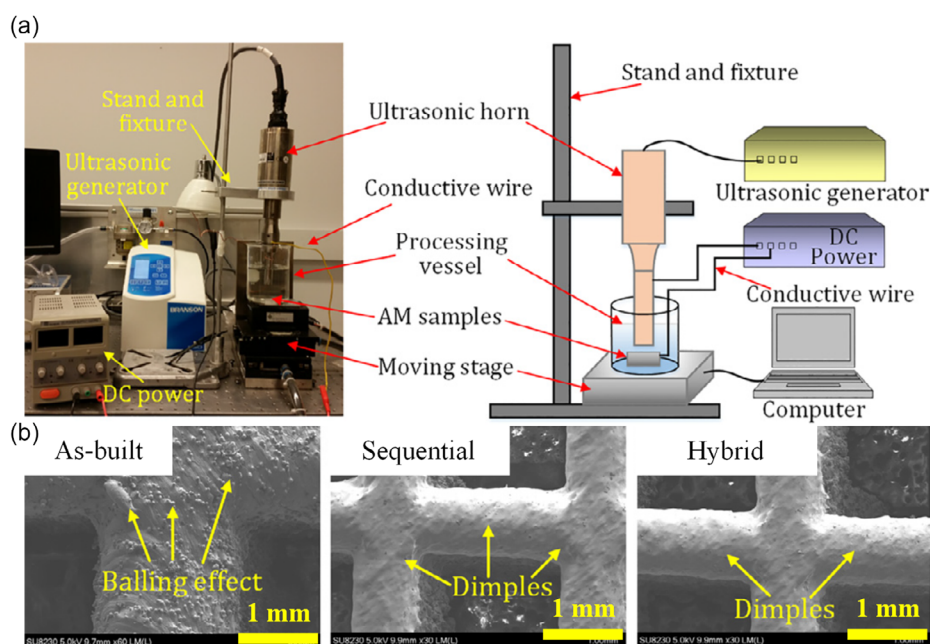


**Figure 21.** a) Experimental setup for hybrid ECP and cavitation peening, b) SEM morphologies of AM lattice structured surfaces before and after post-processing. Adapted with permissions.<sup>[48]</sup> Copyright 2021, Elsevier.



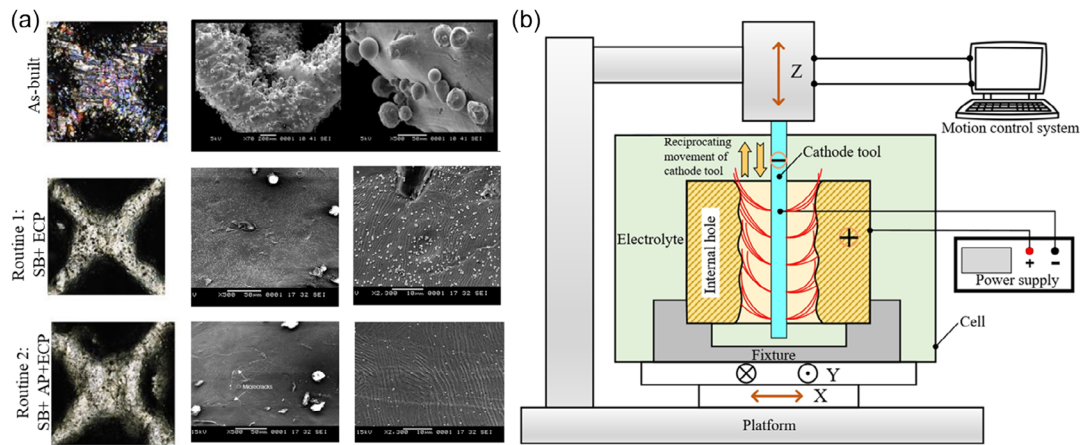


**Figure 22.** a) surface topography following different combinations of sequential post-processing. Adapted under the terms of the CC BY 3.0 license.<sup>[46]</sup> Copyright 2021, The Authors. Published by MDPI. b) Experiment setup of ECMP for the internal hole. Adapted with permissions.<sup>[49]</sup> Copyright 2021, Elsevier.

is reported to be  $5\ \mu\text{m}$  after abrasive polishing, but after ECP it increased to  $12\ \mu\text{m}$ . In conclusion, the final improvement was 20% by post-processing, which was much lower than the first routine. In order to explain this unexpected increase in roughness, pitting corrosion was likely to occur within deep cracks that were created during SB and enlarged during abrasive polishing. **Figure 22a** shows the optical and SEM images before and after the hybrid post-processing. In as-built part, clusters of unmelted particles are visible which were mainly removed by the SB. However, as discussed in Section 5.1 SB can create peel-off layer which was removed by either abrasive polishing or ECP, so no peel-off can be seen in the SEM images after post-processing. After SB + ECP, the microcracks and a large number of foreign particles of Bi were evident. In contrast, after the second treatment routine, there was a widening of internal cavities and fewer residual foreign particles of B, Bi, Si, and Al.<sup>[46]</sup>

In another study by Zhao et al.<sup>[49]</sup> combination of electrochemical and mechanical polishing is used to polish an LB-PBF SS304 internal hole. They have proposed a novel electrochemical mechanical polishing (ECMP) process that is shown in **Figure 22b**. It was very similar to the method in Section 3.2, except that the cathode was designed differently. In this experiment, the cathode electrode was a twisted metal pair and it was covered with a large number of nylon filaments which acted as flexible abrasives. The cathode had a reciprocating movement which enabled scratching the internal surface, releasing gas bubbles and electrolytic products. The ECP was performed using the flow of electrolyte consisting of 10 wt%  $\text{NaNO}_3$  and deionized water at the temperature of  $25\ ^\circ\text{C}$ , inside the machining gap. ECP was performed under constant currents of 2, 5 and  $7\ \text{A cm}^{-2}$ . As a result, the surface roughness of the straight hole was reduced from  $S_a = 14.151\ \mu\text{m}$  to  $S_a = 3.880\ \mu\text{m}$  which is a 72% improvement in surface quality. The mass loss associated with this improvement is 81.4 mg. This improvement was obtained by polishing at the current density of  $7\ \text{A cm}^{-2}$  for 2.86 min. Without the flexible abrasives, this improvement was only 29%.<sup>[49]</sup>

### 6.3. Combination of Mechanical and Chemical

Karami et al.<sup>[24]</sup> have used SB and CP to improve internal and external surface roughness of Ti6Al4V lattice structures produced by LB-PBF. SB was performed for 90 s, with sand particle size  $50\ \mu\text{m}$  under a pressure of 4.5 bar. For CP, two electrolytes were used, the first one was  $50\ \text{mL H}_2\text{O} + 25\ \text{mL HNO}_3 + 5\ \text{mL HF}$  and the CP time of 2 min. The second electrolyte was  $50\ \text{mL H}_2\text{O} + 25\ \text{mL H}_2\text{SO}_4 + 25\ \text{mL HCl}$  and the CP time 60 min. Both chemical treatments are performed under ultrasonic agitation. The second chemical solution (CP2) was less aggressive and safer compared to the first one, which contains HF. The influence of SB and CP on outer and core struts is shown in SEM images in **Figure 23**. According to the results of this study, the combination of SB and CP using a less aggressive solution (**Figure 23a**) was more influential in removing the partially melted particles on both internal and external struts of a lattice structure. By comparing **Figure 23d,f** we can conclude that SB cannot go deep to the core of lattice structure, and we need CP to improve the surface profile of internal struts.<sup>[24]</sup>

Mohammadian et al.<sup>[37]</sup> have used combination of CP and AFP for treatment of an Inconel engine part with an internal edge shape cavity by using flow of a chemical solution. The chemical solution used in this study was 50 vol% HF + 50 vol%  $\text{HNO}_3$  with the flow rate of  $10\ \text{L min}^{-1}$ . Aluminum oxide grit with an average particle size of  $d_{45} = 420\ \mu\text{m}$  and specific gravity of 3.94 was used as the abrasive. Further AFM parameters including abrasive particle concentration in base fluid, volume of polishing media, and flow rate were 6 wt%, 5 L, and  $10\ \text{L min}^{-1}$ , respectively. Pumping pressure was 32.2 psi and polishing times of 1 h. To evaluate the synergistic effect of simultaneously performing abrasive and CP, the time needed to have an 18% decrease in  $R_a$  roughness, from  $R_a = 17.4\ \mu\text{m}$  to  $R_a = 14.2\ \mu\text{m}$  was considered. In order to achieve this result, 8 h of static CP, 3 h of either chemical or AFP, and only 1 h of CP-AFP was required. Therefore, moving from static to chemical flow reduced polishing time by 2.5. In addition, when chemical

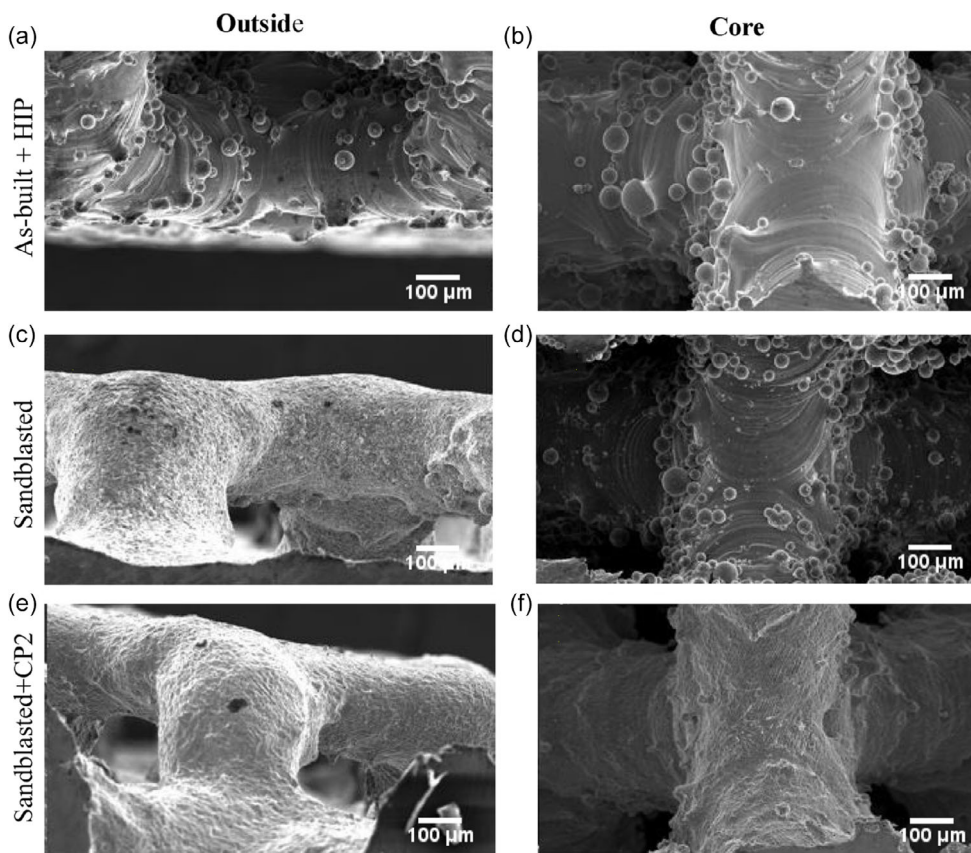


**Figure 23.** The external and internal surface roughness profile of Ti6Al4V lattice structure. a) and b) as-built part after hot isostatic pressing (HIP), c,d) after SB, e,f) after SB + CP (CP2). Adapted under the terms of the CC BY 4.0 license.<sup>[24]</sup> Copyright 2020, The Authors. Published by Elsevier.

and abrasive polishing were combined to replace CP or AFP, the polishing time was reduced by a factor of three.<sup>[37]</sup>

According to the reviewed paper in this section, the combination of different post-processing methods will increase the complexity of the process and require more equipment. However, hybrid methods can produce a smoother surface in less time than individual post-processing and improve experiment performance by a noticeable amount. **Table 6** summarizes the hybrid treatments that were studied, along with their corresponding experimental conditions and the resulting enhancements in roughness.

## 7. Discussion

AM powder-based metallic parts are typically characterized by high surface roughness, due to the layer-by-layer fabrication nature and the physical phenomena during deposition, heating, and solidification. Therefore, post-processing steps are required to achieve the desired surface finish for functional applications of powder-based AM. However, post-processing of complex AM parts, including internal surfaces and inaccessible components, is challenging. In this section, the elaborated post-processing methods (ECP, CP, mechanical polishing, and hybrid methods; see Section 3–6 respectively) used for AM complex parts is

comprehensively discussed here. The present review documented literature published on post-processing of complex AM parts from 2012 to 2024. The primary method utilized to identify relevant literature for this review involved using of the Engineering Village search engine. Engineering Village is a comprehensive abstract and citation database that predominantly focuses on peer-reviewed journals and conference papers. The literature search was conducted using the keywords “post-processing”, “additive manufacturing”, “complex”, “internal-hole”, “internal surface”, “lattice”, “free-form”, “electrochemical polishing”, “chemical polishing”, “abrasive polishing”. This study has classified post-processing methods into four groups: ECP (Section 3), CP (Section 4), mechanical polishing (Section 5), and hybrid methods (Section 6) that combine the first three techniques. The first comparison that is depicted in **Figure 24** discusses the *frequency of use* of each post-processing method (ECP, CP, mechanical and hybrid techniques) applied on complex metallic AM parts. In fact, post-processing methods are applied almost equally for these main four categories and no particular method was privileged on average in the reported AM post-processing use cases.

Another statistical analysis, based on this literature review, compares the average roughness improvement and post-processing time for each distinct post-processing method. According to **Figure 25a**, mechanical methods achieve the

**Table 6.** Summary of polishing experiments using hybrid methods and their performance for AM complex parts.

Material	Basic methods	Experiment details	Time	Roughness improvement (Roughness values are in $\mu\text{m}$ )	Thickness reduction (relative and absolute)	References
Ti6Al4V (lattice)	CP	1% HF + 20% HNO <sub>3</sub>	15 min	46%	3 $\approx$ 4%, 75 $\approx$ 100 $\mu\text{m}$	[21]
	ECP	995 mL ethanol, 100 mL n-butyl alcohol, 109 g of Al(H <sub>2</sub> O) <sub>6</sub> Cl <sub>3</sub> , and 250 g ZnCl <sub>2</sub> , $E = 50\text{ V}$	10 min			
Ti6Al4V (lattice)	CP	0.5 mL HF + 50 g H <sub>2</sub> O	10 min	50% ( $R_a$ : from 12 to 6 $\mu\text{m}$ )	22%, 50 $\mu\text{m}$	[35]
	ECP	55 mL CH <sub>3</sub> COOH + 30 mL H <sub>2</sub> SO <sub>4</sub> + 15 mL HF, $i = 1.2\text{ mA mm}^{-2}$	8 min			
SS 316L (lattice)	ECP	Solution: 42 wt% H <sub>3</sub> PO <sub>4</sub> (with purity of 85 wt%), 47 wt% glycerol, and 11 wt% deionized water, $E = 16\text{ V}$ , $I = 2\text{ A}$ , working distance = 5 mm	10 min	64% ( $S_a$ : from = 9.952 to 3.579 $\mu\text{m}$ )	–	[48]
	Cavitation peening	Frequency = 20 Hz, working distance = 5 mm, Amplitude = 56 $\mu\text{m}$				
SS 316L (lattice)	SB	Peenmatic 750S machine with a nozzle diameter of 5 mm, the working distance of 100–120 mm, pressure range of 60–80 psi, and glass bead diameter of 200–300 $\mu\text{m}$	NA	80% ( $S_a$ : from 15 to 3 $\mu\text{m}$ )	–	[46]
	ECP	90 vol% H <sub>3</sub> PO <sub>4</sub> and H <sub>2</sub> SO <sub>4</sub> at $T =$ of 45–50 °C	10–30 min			
SS 316L (lattice)	SB	Peenmatic 750S machine with a nozzle diameter of 5 mm, the working distance of 100–120 mm, pressure range of 60–80 psi, and glass bead diameter of 200–300 $\mu\text{m}$	NA	20% ( $S_a$ : from 15 to 12 $\mu\text{m}$ )	–	[46]
	AFP	Particle size: SiC, Al <sub>2</sub> O <sub>3</sub> , B <sub>4</sub> C (all less than 10 $\mu\text{m}$ ) and steel grit (150 $\mu\text{m}$ ) with 3 wt%, 4 wt%, 3 wt% and 90 wt%. AP fixed vibration frequency of 30 Hz.	NA			
	ECP	90 vol% H <sub>3</sub> PO <sub>4</sub> and H <sub>2</sub> SO <sub>4</sub> at $T = 45\text{--}50\text{ }^\circ\text{C}$	10–30 min			
SS 304 (internal hole)	ECMP	10 wt% NaNO <sub>3</sub> and deionized water at the $T = 25\text{ }^\circ\text{C}$ Current density = 7 A cm <sup>-2</sup>	2.86 min	72% ( $S_a$ : from 14.151 to 3.880 $\mu\text{m}$ )	81.4 mg	[49]
Ti6Al4V (lattice)	SB	sand particle size 50 $\mu\text{m}$ under a pressure of 4.5 bar	90 s	–	–	[24]
	CP	H <sub>2</sub> O + 25 mL H <sub>2</sub> SO <sub>4</sub> + 25 mL HCl Ultrasonic agitation	60 min			
Inconel 625 (internal hole)	CP	50% HF + 50% HNO <sub>3</sub> , flow rate = 10 L min <sup>-1</sup>	60 min	18% ( $R_a$ : from 17.4 to $R_a = 14.2\text{ } \mu\text{m}$ )	–	[37]
	AFP	Aluminum oxide grit with an average particle size of $d_{45} = 420\text{ } \mu\text{m}$ and specific gravity of 3.94 abrasive particle concentration = 6%, volume of polishing media = 5 L				
Pure Zn (lattice)	CP	5% HCl + 5% HNO <sub>3</sub> + 90% C <sub>2</sub> H <sub>5</sub> OH	20 s	–	17%, 50 $\mu\text{m}$	[82]
	ECP	50% H <sub>3</sub> PO <sub>4</sub> + 50% C <sub>2</sub> H <sub>5</sub> OH at $E = 16\text{ V}$	10 min			
SS 316L (lattice)	CP	3 mL HF + 9 mL HNO <sub>3</sub> + 88 mL H <sub>2</sub> O	3 min	29% ( $R_a$ : from 8.45 to 5.96)	2.1%, 487.80 mg	[44]
	ECP	12 mL H <sub>3</sub> PO <sub>4</sub> + 42 mL C <sub>3</sub> H <sub>8</sub> O <sub>3</sub> + 11 mL H <sub>2</sub> O $E = 12\text{ V}$ , $I = 1.2\text{ A}$ , $T = 75\text{ }^\circ\text{C}$	1.5 min		1.90%, 478.40 mg	

highest improvement in roughness which is 69.9%, followed, in decreasing order, by electrochemical, hybrid, and chemical methods which are 55.5%, 50%, and 49.5% respectively. Considering the processing time, one of the main critical factors for industrial applications, Figure 25b reports, for each category, the average polishing time to achieve an improved surface quality. This figure shows that ECP is the fastest post-processing method,

resulting in an obvious surface finish improvement for complex AM surfaces.

It should be noted that the comparisons illustrated in Figure 25 can be deployed only to preliminary select a post-processing method for a complex AM part. As elaborated in Section 2, each investigated research study has its own methodology and evaluation method; e.g., in some studies, roughness

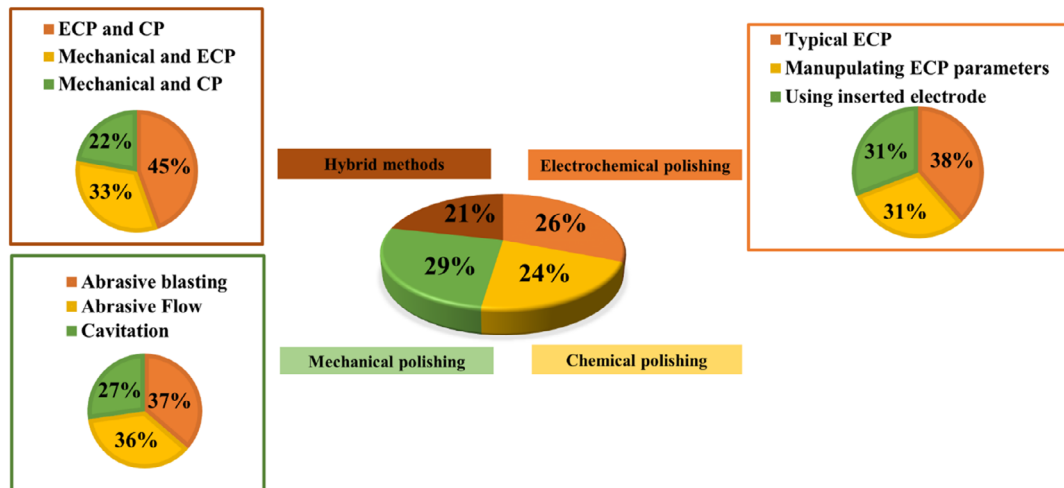


**Figure 24.** Pie charts presenting the proportion of each post-processing method used for AM complex parts.

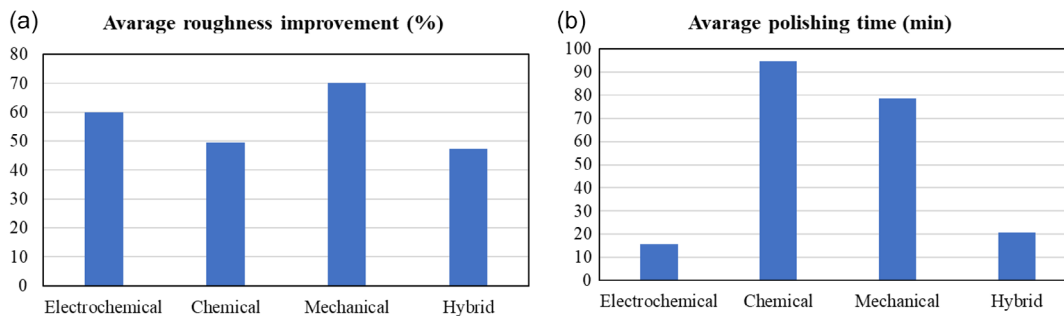


**Figure 25.** a) average roughness improvement and b) average polishing time for different post-processing methods.

measurements were not quantitative and evaluations were done visually by comparing microscope (SEM) images. In addition, not all studies documented the used post-processing parameters. As suggested in Section 2, referencing the standard ASTM F3624 by researchers can address this issue and provide a standardized approach for research articles studying the surface texture of AM parts. Furthermore, it is well-acknowledged by the authors that proper averaging and comparing methods have the highest validity only when the parts' geometry, material, and production methods are identical, with the only variable factor being the post-processing method. I.e., the ideal condition for comparison would involve having a specific complex part made of a particular material and produced with a specific AM machine. Then, different post-processing methods such as ECP, CP, abrasive, and hybrid methods would be applied, and the results would be evaluated. Unfortunately, such a coherent experimental database for different complex parts has not been available until today. Hence, considering the introduced limitation, the presented comparison can still serve as a basic process selection guide, describing the different polishing methods' principles and the criteria for selecting the best post-processing condition.

In this review study, post-processing of different types of AM complex parts, including internal cavities and lattice structures are investigated. In Table 7 the most useful methods for each geometry are reported. Accordingly, it can be witnessed that

mechanical methods are not widely used for lattice parts. During mechanical treatment, high pressure may damage delicate lattice structures. For the parts with internal cavities, chemical and electrochemical methods are more promising. For AM parts including holes, all four post-processing categories seem address internal surface roughness improvement.

The recommendations from this review study for researchers at academia and industry are as follows: 1) There is a lack of agreement in selecting the surface texture parameter and technology for quantifying surface quality improvement through post-processing. It is recommended to utilize the standard ASTM F3624-23 for the selection of appropriate parameters and instruments. 2) As observed in the last column of Table 3–6 of the present review study, more than half of the reviewed literature did not report the amount of material removed by the post-processing. It is important to highlight that the primary goal of AM is net-shape production. Therefore, it is important to quantitatively evaluate the material removal or dimension changes associated with post-processing. While various techniques may yield a smooth surface by removing a significant amount of material, such an outcome is not ideal and can impact the nominal dimensions of the AM part. Thus, it is recommended to simultaneously report both the roughness improvement and the amount of material removed. 3) Despite the significance and growing application of AM complex parts,



**Table 7.** Studied successful application of each categorized post-processing method for specific features in complex metallic (AM) parts, as demonstrated in literature.

	Description of method	Internal hole	Internal cavity	Lattice structure
Electrochemical	General ECP	✓ <sup>[43a]</sup>	✗ <sup>[19]</sup>	✓ <sup>[35,44,71]</sup> ✗ <sup>[21]</sup>
	Manipulated ECP	✓ <sup>[13,20,27]</sup>	–	✓ <sup>[17]</sup>
	Inserted electrode ECP	✓ <sup>[13,17]</sup>	✓ <sup>[19]</sup>	✓ <sup>[50]</sup>
Chemical	CP	–	✓ <sup>[19,37]</sup>	✓ <sup>[24,35,36,38,81,82]</sup>
Mechanical	SB	–	–	✓ <sup>[46]</sup> ✗ <sup>[24,82,85]</sup>
	AFP	–	✓ <sup>[37]</sup>	✗ <sup>[46]</sup>
	AFM	✓ <sup>[47]</sup>	–	–
	Cavitation	✓ <sup>[40–42]</sup>	–	–
Hybrid	CP + ECP	–	–	✓ <sup>[21,35,44,82]</sup>
	ECP+ cavitation	–	–	✓ <sup>[48]</sup>
	SB + ECP	–	–	✓ <sup>[46]</sup>
	SB + AFP + ECP	–	–	✓ <sup>[46]</sup>
	ECMP	✓ <sup>[49]</sup>	–	–
	SB + CP	–	–	✓ <sup>[49]</sup>
	CP + AFP	✓ <sup>[37]</sup>	–	–

<sup>a)</sup> (✓) indicates that the post-processing method listed in the specific row of the table is effective for the geometry described in the corresponding column, (✗) indicates that the specific combination of post-processing and complex geometry does not work, and (–) indicates that there is no available report on that particular combination.

there is insufficient research in the field of their post-processing. While this study has attempted to compile existing knowledge, it remains challenging to ascertain which post-processing method will definitively influence a specific AM complex part with particular dimensions and materials. Therefore, further research in this area is strongly recommended.

## 8. Conclusion

The aim of this review is to investigate the post-processing condition of complex AM parts which has inaccessible surfaces for conventional treatments. The four categories of 1) ECP, 2) CP, 3) mechanical polishing, and 4) hybrid methods, which are combinations of the first three categories, are discussed separately. In each section, post-processing conditions for each research study are described in the text, and a summary is presented in the table at the end of the section. Additionally, the effectiveness of the treatments is assessed by the level of surface roughness improvement or the topographic evolution observed on microscopic images. Based on statistical comparisons presented in the discussion section, we can conclude that: 1) There is only few literature available in this area, hence, the post-processing of complex AM parts are still challenging for industrial applications.

2) Mechanical post-processing methods are not widely used for lattice parts; chemical or electrochemical methods appear to be more promising. 3) CP and ECP methods are most effective for parts with internal cavities. 4) CP removes the attached powder particles, whereas ECP further reduces surface roughness in additive manufactured surfaces. 5) In general, all four categories of post-processing seem to be useful for improving the internal surfaces of AM holes.

## Acknowledgements

This work was supported by the Natural Sciences and Engineering Research Council of Canada (NSERC) under the Discovery grant (RGPIN-2019-05973).

## Conflict of Interest

The authors declare no conflict of interest.

## Keywords

additive manufacturing, chemical polishing, complex geometry, electrochemical polishing, lattice structure, mechanical polishing, post-processing

Received: September 18, 2023

Revised: March 5, 2024

Published online:

- [1] ASTM ISO 52900-21 Additive Manufacturing — General Principles — Fundamentals and Vocabulary **2021**.
- [2] W. J. Sames, F. A. List, S. Pannala, R. R. Dehoff, S. S. Babu, *Int. Mater. Rev.* **2016**, *61*, 315.
- [3] E. Matias, B. Rao, in *Portland Int. Conf. on Management of Engineering and Technology 2015*, Portland, OR, September **2015**, p. 551.
- [4] O. Ivanova, C. Williams, T. Campbell, *Rapid Prototyp J.* **2013**, *19*, 353.
- [5] S. Mirzababaei, S. Pasebani, *J. Manuf. Mater. Process.* **2019**, *3*, 8.
- [6] W. Han, F. Fang, *Int. J. Mach. Tools Manuf.* **2019**, *139*, 1.
- [7] L. E. J. Thomas-Seale, J. C. Kirkman-Brown, M. M. Attallah, D. M. Espino, D. E. T. Shepherd, *Int. J. Prod. Econ.* **2018**, *198*, 104.
- [8] L. W. Hunter, D. Brackett, N. Brierley, J. Yang, M. M. Attallah, *Int. J. Adv. Manuf. Technol.* **2020**, *106*, 4521.
- [9] R. Singh, A. Gupta, O. Tripathi, S. Srivastava, B. Singh, A. Awasthi, S. K. Rajput, P. Sonia, P. Singhal, K. K. Saxena, *Mater. Today Proc.* **2020**, *26*, 3058.
- [10] D. Svetlizky, M. Das, B. Zheng, A. L. Vyatskikh, S. Bose, A. Bandyopadhyay, J. M. Schoenung, E. J. Lavernia, N. Eliaz, *Mater. Today* **2021**, *49*, 271.
- [11] M. Li, W. Du, A. Elwany, Z. Pei, C. Ma, *J. Manuf. Sci. Eng.* **2020**, *142*, 1.
- [12] V. M. S. Muthaiah, S. Indrakumar, S. Suwas, K. Chatterjee, *Bioprinting* **2022**, *25*, e00180.
- [13] H. Fayazfar, I. Rishmawi, M. Vlasea, *J. Mater. Eng. Perform.* **2021**, *30*, 2245.
- [14] F. Calignano, *Virtual Phys. Prototyp.* **2018**, *12*, 97.
- [15] E. Maleki, S. Bagherifard, M. Bandini, M. Guagliano, *Addit. Manuf.* **2021**, *37*, 101619.
- [16] T. M. Mower, M. J. Long, *Mater. Sci. Eng. A* **2016**, *651*, 198.
- [17] S. Chang, A. Liu, C. Y. A. Ong, L. Zhang, X. Huang, Y. H. Tan, L. Zhao, L. Li, J. Ding, *Mater. Res. Lett.* **2019**, *7*, 282.

- [18] J. Mingear, B. Zhang, D. Hartl, A. Elwany, *Addit. Manuf.* **2019**, 27, 565.
- [19] P. Tyagi, T. Goulet, C. Riso, R. Stephenson, N. Chuenprateep, J. Schlitzer, C. Benton, F. Garcia-Moreno, *Addit. Manuf.* **2019**, 25, 32.
- [20] U. Ali, H. Fayazfar, F. Ahmed, E. Toyserkani, *Vacuum* **2020**, 177, 109314.
- [21] G. Dong, J. Marleau-Finley, Y. F. Zhao, *Int. J. Adv. Manuf. Technol.* **2019**, 104, 3401.
- [22] E. S. Gadelmawla, M. M. Koura, T. M. A. Maksoud, I. M. Elewa, H. H. Soliman, *J. Mater. Process. Technol.* **2002**, 123, 133.
- [23] J. Leitão, T. Hegdahl, *Acta Odontol. Scand.* **2009**, 39, 379.
- [24] K. Karami, A. Blok, L. Weber, S. M. Ahmadi, R. Petrov, K. Nikolic, E. V. Borisov, S. Leeflang, C. Ayas, A. A. Zadpoor, M. Mehdipour, E. Reinton, V. A. Popovich, *Addit. Manuf.* **2020**, 36, 101433.
- [25] L. Wiesent, U. Schultheiß, P. Lulla, U. Noster, T. Schratzenstaller, C. Schmid, A. Nonn, A. Spear, *PLoS One* **2020**, 15, 1.
- [26] R. Singh, N. B. Dahotre, *J. Mater. Sci. Mater. Med.* **2007**, 18, 725.
- [27] U. Su Kim, J. Woo Park, *Int. J. Precis. Eng. Manuf.-Green Technol.* **2019**, 6, 11.
- [28] Y. Zhang, J. Li, S. Che, Y. Tian, *Met. Mater. Int.* **2020**, 26, 783.
- [29] Y. C. Wu, C. N. Kuo, Y. C. Chung, C. H. Ng, J. C. Huang, *Materials* **2019**, 12, 1466.
- [30] X. Peng, L. Kong, J. Y. H. Fuh, H. Wang, *J. Manuf. Mater. Process.* **2021**, 5, 38.
- [31] N. N. Kumbhar, A. V. Mulay, *J. Inst. Eng.: C* **2018**, 99, 481.
- [32] S. Mazo, A. Thompson, L. Newton, R. Leach, *Metrology* **2023**, 3, 237.
- [33] ISO 21920-2 Geometrical Product Specification (GPS):Surface Texture: Profile, Part 2: Terms, Definitions and Surface Texture Parameters **2021**.
- [34] ISO 25178-2 Geometrical Product Specifications (GPS) Surface Texture: Areal, Part 2: Terms, Definitions and Surface Texture Parameters **2021**.
- [35] G. Pyka, A. Burakowski, G. Kerckhofs, M. Moesen, S. Van Bael, J. Schrooten, M. Wevers, *Adv. Eng. Mater.* **2012**, 14, 363.
- [36] G. Pyka, G. Kerckhofs, I. Papantoniou, M. Speirs, J. Schrooten, M. Wevers, *Materials* **2013**, 6, 4737.
- [37] N. Mohammadian, S. Turenne, V. Brailovski, *J. Mater. Process. Technol.* **2018**, 252, 728.
- [38] C. de Formanoir, M. Suard, R. Dendievel, G. Martin, S. Godet, *Addit. Manuf.* **2016**, 11, 71.
- [39] C. W. Kum, C. H. Wu, S. Wan, C. W. Kang, *J. Mater. Process. Technol.* **2020**, 282, 116704.
- [40] A. P. Nagalingam, S. H. Yeo, *Addit. Manuf.* **2020**, 36, 101428.
- [41] A. P. Nagalingam, S. H. Yeo, *Wear* **2018**, 414–415, 89.
- [42] A. P. Nagalingam, H. K. Yuvaraj, S. H. Yeo, *Addit. Manuf.* **2020**, 33, 101110.
- [43] D. Jiang, Y. Tian, Y. Zhu, A. Huang, *Surf. Coat. Technol.* **2022**, 441, 128529.
- [44] E. Langi, L. G. Zhao, P. Jamshidi, M. Attallah, V. V. Silberschmidt, H. Willcock, F. Vogt, *Mater. Today Commun.* **2022**, 31, 103372.
- [45] A. G. Demir, B. Previtali, *Mater. Des.* **2017**, 119, 338.
- [46] A. Q. A. Teo, L. Yan, A. Chaudhari, G. K. O'Neill, *Materials* **2021**, 14, 1.
- [47] S. Han, F. Salvatore, J. Rech, J. Bajolet, *Precis. Eng.* **2020**, 64, 20.
- [48] B. Wang, J. Castellana, S. N. Melkote, *CIRP Ann.* **2021**, 70, 175.
- [49] C. Zhao, N. Qu, X. Tang, *J. Manuf. Process.* **2021**, 64, 1544.
- [50] M. E. Lynch, K. Williams, M. Cabrera, T. Beccuti, *Int. J. Adv. Manuf. Technol.* **2021**, 113, 967.
- [51] ASTM F3624-23 Standard Guide for Additive Manufacturing of Metals - Powder Bed Fusion - Measurement and Characterization of Surface Texture **2023**.
- [52] C. Y. Poon, B. Bhushan, *Wear* **1995**, 190, 76.
- [53] E. C. Teague, F. E. Scire, S. M. Baker, S. W. Jensen, *Wear* **1982**, 83, 1.
- [54] Z. Yilbas, M. S. J. Hasmi, *J. Mater. Process. Technol.* **1999**, 88, 10.
- [55] D. J. Whitehouse, *CIRP Ann.* **1988**, 37, 649.
- [56] R. Danzl, F. Helmlí, S. Scherer, *The 10th Inter. Conf. of the Slovenian Society for Non-Destructive Testing, Citeseer* **2009**, p. 484.
- [57] W. J. Stemp, D. A. Macdonald, M. A. Gleason, *J. Archaeol. Sci. Rep.* **2019**, 24, 513.
- [58] C. Sheppard, D.S.-(No Title), undefined 1997, *Cir.Nii.Ac.Jp* n.d.
- [59] G. Kerckhofs, G. Pyka, M. Moesen, S. Van Bael, J. Schrooten, M. Wevers, *Adv. Eng. Mater.* **2013**, 15, 153.
- [60] N. Vanderesse, P. Bocher, N. Nuño, A. Yáñez, L. A. Hof, *Addit. Manuf.* **2022**, 54, 102731.
- [61] A. Townsend, L. Pagani, P. Scott, L. Blunt, *Precis. Eng.* **2017**, 48, 254.
- [62] N. Senin, A. Thompson, R. K. Leach, *Meas. Sci. Technol.* **2017**, 28, 095003.
- [63] C. Gomez, R. Su, A. Thompson, J. DiSciaccia, S. Lawes, R. K. Leach, *Opt. Eng.* **2017**, 56, 111714.
- [64] ASTM B374 – 06 Standard Terminology Relating to Electroplating **2019**.
- [65] L. E. A. Berlouis, D. J. Schiffrin, *Trans. IMF* **2017**, 63, 52.
- [66] D. Landolt, *Electrochim. Acta* **1987**, 32, 1.
- [67] M. Datta, D. Landolt, *Electrochim. Acta* **2000**, 45, 2535.
- [68] D. Kim, K. Son, D. Sung, Y. Kim, W. Chung, *Corros. Sci.* **2015**, 98, 494.
- [69] O. Rodríguez-Martínez, L. M. Martínez, M. Videa, *J. Nanopart. Res.* **2020**, 22, 1.
- [70] P. B. Tailor, A. Agrawal, S. S. Joshi, *Int. J. Mach. Tools Manuf.* **2013**, 66, 15.
- [71] S. A. Tyagi, M. Manjaiah, *Mater. Today Commun.* **2024**, 38, 108267.
- [72] S. J. Lee, Y. H. Chen, J. C. Hung, *Int. J. Electrochem. Sci.* **2012**, 7, 12495.
- [73] W. Han, F. Fang, *J. Manuf. Sci. Eng. Trans. ASME* **2019**, 141, 101015.
- [74] P. S. Pa, H. Hocheng, *Int. J. Adv. Manuf. Technol.* **2006**, 34, 517.
- [75] H. Hocheng, P. S. Pa, *Int. J. Adv. Manuf. Technol.* **2003**, 21, 995.
- [76] *Extrude Hone - Deburring - Polishing - Radiusing, Shaping - Flow Tuning* n.d.
- [77] S. Patel, A. Rogalsky, M. Vlasea, *J. Mater. Res.* **2020**, 35, 2055.
- [78] V. Candela, M. Pozzi, E. Chyhyrynets, V. Garcia Diaz, S. Candela, R. Dima, G. Favero, C. Pira, A. Pepato, P. Sonato, *Int. J. Adv. Manuf. Technol.* **2022**, 123, 3205.
- [79] T. Peng, K. Kellens, R. Tang, C. Chen, G. Chen, *Addit. Manuf.* **2018**, 21, 694.
- [80] B. Wysocki, J. Idaszek, K. Szlajak, K. Strzelczyk, T. Brynk, K. J. Kurzydłowski, W. Świeszkowski, *Materials* **2016**, 9, 197.
- [81] B. Wysocki, J. Idaszek, J. Buhagiar, K. Szlajak, T. Brynk, K. J. Kurzydłowski, W. Świeszkowski, *Mater. Sci. Eng. C* **2019**, 95, 428.
- [82] P. Wen, Y. Qin, Y. Chen, M. Voshage, L. Jauer, R. Poprawe, J. H. Schleifenbaum, *J. Mater. Sci. Technol.* **2019**, 35, 368.
- [83] B. K. Gale, M. A. Eddings, S. O. Sundberg, A. Hatch, J. Kim, T. Ho, S. M. Karazi, *Reference Module in Materials Science and Materials Engineering*, Elsevier, Amsterdam **2016**.
- [84] Y. Wang, Z. Zhu, J. Liu, H. Zhang, Y. Liu, J. Yuan, J. C. Balza, D. Zujur, L. Gil, R. Subero, E. Dominguez, P. Delvasto, J. Alvarez, *IOP Conf. Ser. Mater. Sci. Eng.* **2013**, 45, 012004.
- [85] S. M. Ahmadi, R. Kumar, E. V. Borisov, R. Petrov, S. Leeflang, Y. Li, N. Tümer, R. Huizenga, C. Ayas, A. A. Zadpoor, V. A. Popovich, *Acta Biomater.* **2019**, 83, 153.
- [86] S. S. Kumar, S. S. Hiremath, *Procedia Technol.* **2016**, 25, 1297.
- [87] V. K. Gorana, V. K. Jain, G. K. Lal, *Wear* **2006**, 260, 128.

- [88] L. Rhoades, *J. Mater. Process. Technol.* **1991**, *28*, 107.  
[89] L. Yin, K. Ramesh, S. Wan, D. Liu, H. Huang, Y. C. Liu, *Mater. Manuf. Process.* **2004**, *19*, 187.  
[90] P. Tyagi, D. Brent, T. Saunders, T. Goulet, C. Riso, K. Klein, F. G. Moreno, *Int. J. Adv. Manuf. Technol.* **2020**, *106*, 1337.

- [91] Surface Roughness Measurement—Parameters | Olympus, [https://www.olympus-ims.com/en/metrology/surface-roughness-measurement-portal/parameters/#!cms\[focus\]=cmsContent14709](https://www.olympus-ims.com/en/metrology/surface-roughness-measurement-portal/parameters/#!cms[focus]=cmsContent14709) (accessed: February 2024).  
[92] W. Demisse, J. Xu, L. Rice, P. Tyagi, *Prog. Addit. Manuf.* **2023**, *8*, 1433.



**Shamim Pourrahimi** obtained her M.Sc. in materials engineering from Amirkabir University of Technology (Tehran Polytechnic). Currently, she is pursuing her Ph.D. in the Department of Mechanical Engineering at École de technologie supérieure (ÉTS). The main focus of her Ph.D. research is on the optimization of electrochemical polishing and chemical post-processing methods for complex additive-manufactured parts, as well as studying the influence of these post-processing techniques on their corrosion behavior.



**Lucas A. Hof**, ing., Ph.D., is an associate professor in the Mechanical Engineering Department at École de technologie supérieure, Canada. He obtained his Ph.D. in Mechanical Engineering at Concordia University and both his Masters and Bachelor in Mechanical Engineering at Delft University of Technology. His research evolves from the need of a transformation from linear to circular manufacturing practices and concentrates on developing smart remanufacturing technologies for ceramic, metallic and polymer composite materials. Prof. Hof has expertise on advanced manufacturing and materials science with a focus on sustainable production using industry 4.0 technologies, such as artificial intelligence and additive manufacturing.